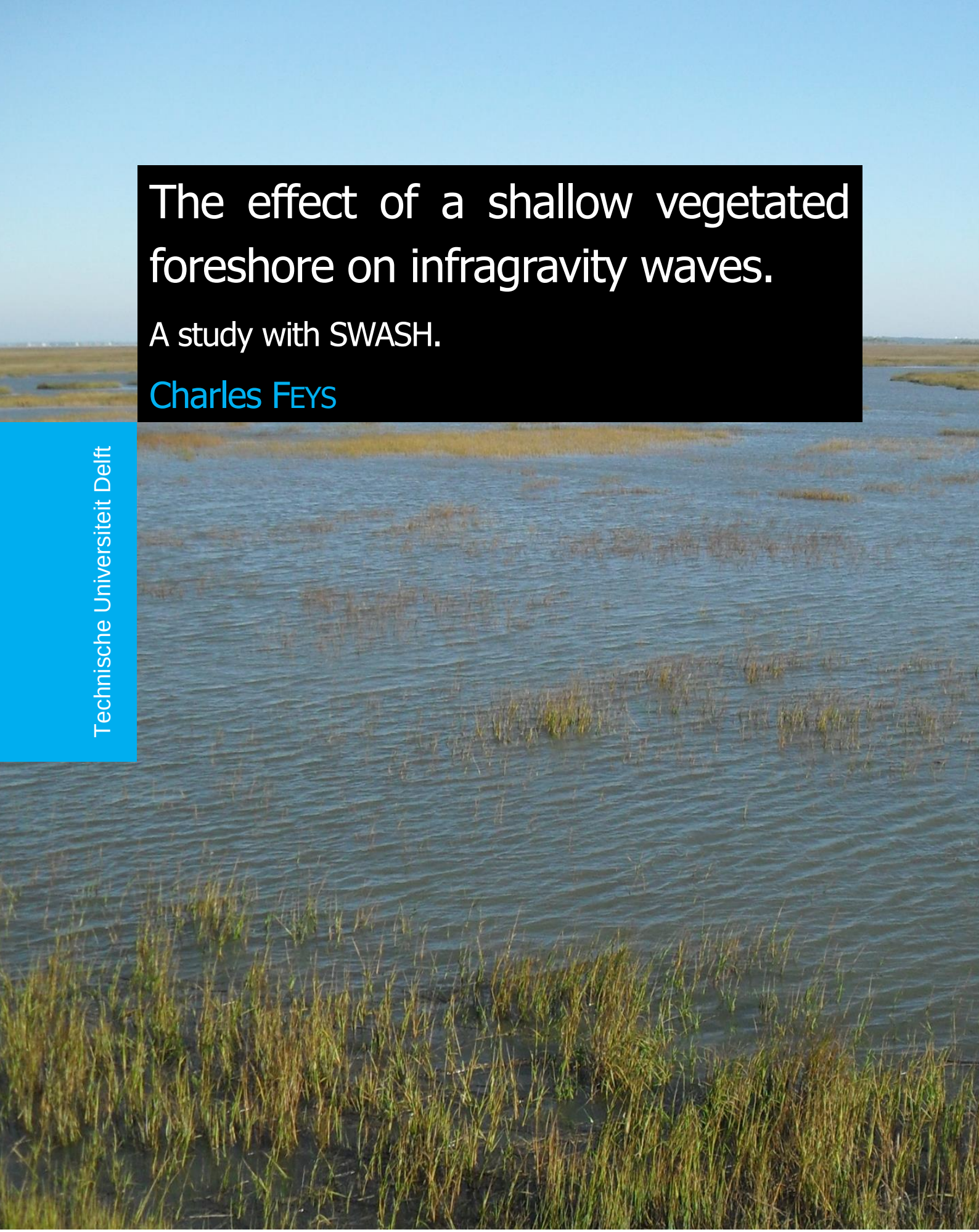

The effect of a shallow vegetated foreshore on infragravity waves.

A study with SWASH.

Charles FEYS

Technische Universiteit Delft

TU Delft Delft University of Technology

CoMEM

The effect of a shallow vegetated foreshore on infragravity waves.

A study with SWASH.

By

Charles FEYS

in partial fulfilment of the requirements for the degree of

Master of Science

In Coastal & Marine Engineering and Management

at the Delft University of Technology,

to be defended publicly on Wednesday July 18, 2018 at 08:30 AM.

Thesis committee:

Prof. dr. ir. A.J.H.M. Reniers, TU Delft

Dr. ir. J.D. Bricker, TU Delft

Dr. M.E.S. Tissier, TU Delft

Ir. C.H. Lashley, PhD, TU Delft

Dr. Ir. C. Ferreira, George Mason University

TU Delft

ERASMUS +: ERASMUS MUNDUS MOBILITY PROGRAMME

Master of Science in

COASTAL AND MARINE ENGINEERING AND MANAGEMENT

CoMEM

THE EFFECT OF A SHALLOW VEGETATED FORESHORE ON INFRAGRAVITY WAVES.

A STUDY WITH SWASH.

Technische Universiteit Delft
18 July 2018

Charles FEYS

The Erasmus+: Erasmus Mundus MSc in Coastal and Marine Engineering and Management is an integrated programme including mobility organized by five European partner institutions, coordinated by Norwegian University of Science and Technology (NTNU).

The joint study programme of 120 ECTS credits (two years full-time) has been obtained at two or three of the five CoMEM partner institutions:

- Norges Teknisk- Naturvitenskapelige Universitet (NTNU) Trondheim, Norway
- Technische Universiteit (TU) Delft, The Netherlands
- Universitat Politècnica de Catalunya (UPC). BarcelonaTech. Barcelona, Spain
- University of Southampton, Southampton, Great Britain
- City University London, London, Great Britain

During the first three semesters of the programme, students study at two or three different universities depending on their track of study. In the fourth and final semester an MSc project and thesis has to be completed. The two-year CoMEM programme leads to a multiple set of officially recognized MSc diploma certificates. These will be issued by the universities that have been attended by the student. The transcripts issued with the MSc Diploma Certificate of each university include grades/marks and credits for each subject.

Information regarding the CoMEM programme can be obtained from the programme coordinator:

Øivind A. Arntsen, Dr.ing.
Associate professor in Marine Civil Engineering
Department of Civil and Environmental Engineering
NTNU Norway

Mob.: +4792650455 Fax: + 4773597021

Email: oivind.arntsen@ntnu.no

CoMEM URL: https://www.ntnu.edu/studies/mscomem

CoMEM Thesis

This thesis was completed by:

Charles FEYS

Under supervision of:

Prof. dr. ir. A.J.H.M. Reniers, TU Delft

Dr. ir. J.D. Bricker, TU Delft

Dr. M.E.S. Tissier, TU Delft

Ir. C.H. Lashley, PhD, TU Delft

Dr. Ir. C. Ferreira, George Mason University

As a requirement to attend the degree of

Erasmus+: Erasmus Mundus Master in Coastal and Marine Engineering and Management (CoMEM)

Taught at the following educational institutions:

Norges Teknisk- Naturvitenskapelige Universitet (NTNU)

Trondheim, Norway

Technische Universiteit (TU) Delft

Delft, The Netherlands

University of Southampton,

Southampton, Great Britain

At which the student has studied from August 2016 to July 2018.

Abstract

A specific type of wave is identified as an infragravity wave (IG wave). These waves with very long wave periods, even up to minutes, are possibly dangerous for flood events, increased storm surge and/or failure of coastal defences. Current guidelines for dike safety are often determined for gravity wave dominated systems, so identifying IG dominated systems can be a tool to determine whether dike safety guidelines are sufficient or not.

To analyse the IG waves, the non-hydrostatic simulation model SWASH is proposed. An extensive model validation was carried out, comparing the results of a lab experiment with the model output to assess the model's accuracy to simulate the IG waves. Next, four parameters were chosen to be varied (offshore wave height and period, beach slope and vegetation type) to create several scenarios, mimicking real-life situations in the Wadden Sea and the Chesapeake Bay. To express the IG wave dominance, the Infragravity coefficient (IGC) is used, which is the low-frequency over the high-frequency wave height ratio. IG dominance is defined when the IGC>1.0, and a very IG dominant system is defined when IGC>2.0. For this study, the IGC is analysed at a dike toe.

The effect of a slope on IG dominance shows that weak slopes (1:500) show very IG dominance overall, no matter the offshore conditions. As the slope gets steeper, the gravity waves start to dominate, starting at the lower wave heights. The wave heights show almost never IG dominance for low values (1m) and show more IG dominance as the offshore wave height increases. The offshore period has a minimal influence on IG dominance for short periods, but the IGC seems to decrease after an offshore period of 10s. This effect is mostly visible on steep slopes, and barely visible for weak slopes.

When vegetation is added to the weak-sloped scenario (1:500), it is concluded that vegetation dissipates both the low -and high-frequency wave heights in case of low offshore wave heights (1 and 2m) and short periods (6 and 8s). For higher and longer waves, vegetation dissipates high-frequency gravity waves better than low-frequency IG waves. This shows an increase in IG dominance with the inclusion of vegetation. For very high and long waves (10m, 14s) the vegetation's effect is minimal.

These results from this study show that for a large number of scenarios, mainly for weak slopes, IG waves dominate over gravity waves.

Keywords: CoMEM, infragravity dominance, infragravity waves, nature-based flood defences, numerical modelling, non-hydrostatic simulation, SWASH, vegetation.

Acknowledgements

This thesis is the final work to complete the Master of Science in Coastal and Marine Engineering and Management (CoMEM). During this program, three universities were visited: the Norwegian University of Science and Technology (NTNU), Delft University of Technology (TU Delft) and the University of Southampton.

I would like to start this acknowledgement by thanking my whole thesis committee, with special thanks to Ad Reniers for accepting the position as my committee chair, despite his busy schedule and my limited time to complete this work. I would like to thank my daily supervisors Jeremy Bricker, Chris Lashley and Marion Tissier, for giving me their advice, ideas and guidance. Next, Celso Ferreira for providing the Chesapeake Bay data and despite the distance and time difference, following my progress. Some special thanks go to Marcel Zijlema and Toni Glasbergen for guiding me throughout the SWASH learning process.

My warmest thanks go out to Øivind Arntsen and Sonja Marie Ekrann Hammer, for organising the two-year study program CoMEM and making sure we all felt at home in our first semester in Trondheim.

I would like to thank my family to keep following my progress during these two years and to come to visit me in Delft. Special thanks go to my mom for financing this whole study, for always supporting me and for listening to me endlessly talking about waves. Thank you to all my friends back home for keeping in contact with me while I was away and for making time during my limited visits back to Belgium. Furthermore, I would like to thank my team mates in the Southampton Skunks and Force Elektro Delft, for welcoming me into their teams and for showing me a sport I really enjoy.

Most of all, I would love to thank my fellow CoMEM students, for all the friendship, happiness and love during these unforgettable two years of adventure. For all our big and small journeys around the world, for all our nights out and nights in, for a beautiful mix of people that made the best group of friends I could ever imagine.

Finally, I would like to thank everyone I met in Trondheim, Delft and Southampton to make this experience so memorable.

Charles Feys
Delft, July 2018

Table of contents

List of Figures

List of Tables

List of Abbreviations

IG	Infragravity
IGC	Infragravity Coefficient
JONSWAP	Joint North Sea Wave Project
MWL	Mean Water Level
RMSE	Root Mean Squared Error
SCI	Scatter Index
SIDS	Small Island and Developing States
SWASH	Simulating Waves till Shore

List of Symbols

a	Amplitude	m
b_v	Plant stem diameter	m
C_D	Drag coefficient	-
c_g	Group velocity	m/s
f	Frequency	Hz
L	Wave length	m
g	Gravitational acceleration	m/s^2
H_{m0}	Significant wave height	m
$H_{m0, LF}$	Low frequency wave height	m
$H_{m0, HF}$	High frequency wave height	m
h	Water depth	m
k	Wave number	1/m
Re	Reynolds number	-
S_{xx}	Radiation shear stress	N/m^2
T_P	Wave peak period	s
u_{max}	Maximum horizontal particle velocity	m/s
α	Sea bed slope	-
β_s	Normalized bed slope parameter	-
η	Surface elevation	m
ν	kinematic viscosity	m^2/s
ξ	Iribarren number	-
ρ	Density	Kg/m^3
ω	Radial frequency	1/m

1. Introduction

1.1. Background

Floods can be the most destructive of all natural disasters (United Nations, 2004). It also happens that about 37 percent of the world lives within 100km of the coast, and by 2030, about half of the world population would live within 100km of a coast (Brooks, Nicholls and Haii, 2006). Such environments have clear ecosystem services, such as provisioning of food and water, recreational and cultural values, natural protection, but also the presence of large international ports and trade routes (Millennium Ecosystem Assessment, 2005). With this rich and increasing activity, protecting the coasts from floods and limiting flood risk is therefore vital.

Flood risk consists of two elements: the probability that the flood would happen and the consequences of the flood (economic, social, environmental, …), therefore flood risks can be simply formulated as 'risk = probability × consequence' (CIRIA, 2013). From this, two different cases can be determined. For one where the probability is high, so where flood defence is less developed as it should be, mainly in Small Island Developing States (SIDS), with storms such as the typhoon Haiyan in 2013 in the Philippines (Roeber and Bricker, 2015) and hurricanes Sandy and Harvey in the Caribbean in 2012 and 2017. There is another side to the story, not only the probability can be high, but also the consequences of a coastal storm could be enormous, in other words at coastal megacities, or cities with over 10 million inhabitants (United Nations, 2016). The consequences of a flood at those megacities could be catastrophic, as has been proven in the past by hurricane Sandy in New York in 2012 (Hatzikyriakou *et al.*, 2016), and typhoon Winnie in Shanghai in 1997 (Xian *et al.*, 2018).

Figure 1. Megacities in 2016 and vulnerable SIDS. Image adapted from *(Nicholls, Hoozemans and Marchand, 1999; United Nations, 2016; Scandurra* et al., *2018).*Figure 1 shows both the megacities and the SIDS in the world. Some vulnerable regions are the South Pacific Ocean, the Gulf of Mexico and the Indian Ocean. From all 31 current megacities, 19 of those are located directly on a coast.

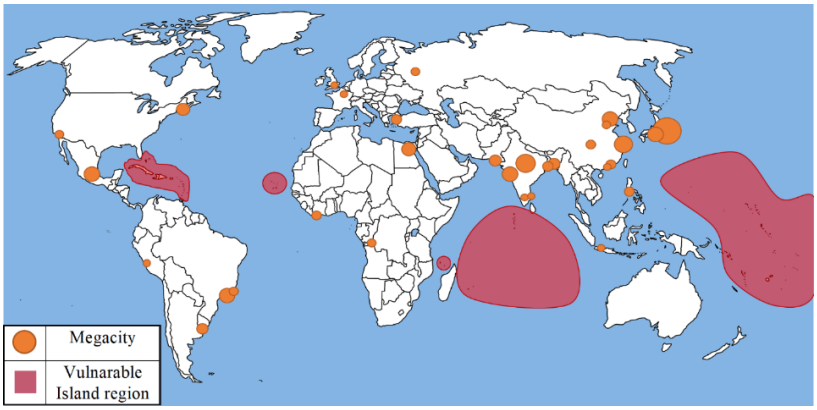

Figure 1. Megacities in 2016 and vulnerable SIDS. Image adapted from (Nicholls, Hoozemans and Marchand, 1999; United Nations, 2016; Scandurra *et al.*, 2018).

1.1.1. Waves

This research will focus on flood due to waves. Therefore, it is important to understand how a wave progresses to shore and what parameter of the wave actually causes the flood. Coasts are expected to be protected from wave impacts, even extreme events. Given that the flood protection doesn't breach, the land behind the protection can still be flooded.

When waves travel to shore, they will usually break in the surf zone and their energy dissipates. Not all energy though, a segment of that energy is converted into potential energy and manifests physically as run-up on the foreshore (Stockdon *et al.*, 2006). Run-up is the water level elevation on the shore due to waves, measured from the still water level. During an average wave climate, this is usually not a problem. The interest here lays in the storm events. During these storms, the water level elevation on the coast can rise to extreme levels and will be problematic in several cases, such as overtopping and erosion. The run-up is divided into two parameters: a time-averaged elevation called 'set-up' and a fluctuating part called 'swash'. A specific type of wave that enlarges the problem of run-up is the infragravity (IG) wave (Bertin *et al.*, 2018). It is a very long wave with a small amplitude that is bound to a wave group but wouldn't break with the rest of the group. Therefore, it could continue to travel through the surf zone and onto the shore. The IG waves can be very dangerous and problematic, although they cannot be observed with the naked eye like short waves.

1.1.2. The Netherlands

The Netherlands is an active country in research and gathering knowledge of flood risk and protection. In calculation formulas such as overtopping and runup, gravity waves are well accounted for (Van der Meer *et al.*, 2016). However, in the past few years, IG waves have been given more attention (Bertin *et al.*, 2018) but are not implemented in these formulas. One reason is because the effects of these waves are not perfectly known yet. If considered significant, they could mean an increased flood risk. To counter these unknowns, the Dutch Flood Protection program (HWBP) introduced the 'All Risk' program in 2014 (STW, 2016). One of its goals is to improve risk management with cutting-edge scientific knowledge in, amongst others, the field of hydraulics. Within this framework, understanding IG waves better and assessing their effects on flood defences is an important step. Calculation software is already available to simulate IG waves, known as phase-resolving software. The next step on this topic is the validation of such software, with an attempt to identify IG waves and where they break (or don't break).

1.1.3. Nature-based flood defence

Coasts need to be protected. As mentioned before, many of the world's megacities are located on the coast. Although this gives a lot of social and economic advantages, it has often negative effects on the environmental aspects, such as the loss of all kinds of natural systems, such as wetlands (Nicholls, 2004), coral reefs (Hedberg *et al.*, 2017) and mangroves (Tuholske *et al.*, 2017).

An active discussion these days is the effect of vegetation on wave dissipation. It has been proven on multiple occasions that natural systems can work as flood protection (Dean and Bender, 2006; US Army Corps of Engineers, 2015; van der Nat *et al.*, 2016; Vuik *et al.*, 2016). Few researches exist up to now about the effects of vegetation, especially salt marshes, on IG waves. Researches combining IG waves with mangroves (Hewageegana *et al.*, 2017) or reefs (Su and Ma, 2018) are more common.

1.2. Problem definition

As briefly introduced, the motivations for this thesis are as following:

- Floods are a worldwide risk. Wave-induced floods can only be countered if fully understood.
- IG waves are an important part of wave run-up and need more research.
- The conditions in which IG waves are dominant are currently not perfectly understood.
- Nature-based approaches as a flood defence can possibly bring a lot of advantages, but the general understanding needs improvement.

Using this information, the problem statement can be defined as:

"Equations to predict and/or calculate overtopping, run-up, dike safety, … assume situations where gravity waves dominate. However, IG waves are known to influence the situation near-shore and could be an important factor to determine dike safety. Identifying IG waves, or selecting which conditions increase/decrease the occurrence of IG waves is very useful for flood prediction.

Many of the coastal areas are vegetated. With the rising popularity of soft coastal defences, it is important to know the effects of vegetation on waves, more specific on IG waves. The effects of coastal wetlands on these IG waves have little research and need to be better understood."

1.3. Objective

The objective of this thesis is to figure out in what situations IG waves dominate over gravity waves.

This is done by simulating different scenarios in which IG waves occur and to analysing the effects of varying different parameters on IG waves, by means of a numerical study using the software SWASH. The varying parameters are chosen as follows:

- Offshore wave height H_{m0},
- Offshore peak period T_P,
- Beach slope, and
- Vegetation type.

The combinations of these give a great number of scenarios to be simulated. Therefore, it is needed to find an optimal way of doing this in the simulation software SWASH.

1.4. Research question

To guide this thesis, the following research question is posed:

"Under what combinations of topography, vegetation and offshore conditions do infragravity waves dominate at a dike toe?"

Although this is the focus of this research, some secondary research questions are set:

- What is the optimal run-time versus accuracy equilibrium in SWASH to simulate a large number of scenarios in shallow environment?
- What is a suitable parameter to analyse the magnitude and/or dominance of infragravity waves over a foreshore.
- What is the effect of different kinds of vegetation on infragravity waves?

1.5. Significance of this research

This research should contribute to the general body of knowledge about the topic. Here are some indications concerning the significance of the research.

1.5.1. Novel aspects

In addition, this research is significant for the general body of knowledge in the following few aspects:

1. Although the IG wave is already understood well, some aspects are still uncertain. For example, its dominance over gravity waves during storm events.

2. Using vegetation as a storm protection is being assessed more and more these days. The combination of IG waves and coastal wetlands has for now been researched very little.
3. The assessment of the changes of IG waves under different conditions is important to know for the future changes to overtopping and run-up formulas. In this research, several parameters are modified systematically based on real-life conditions.

1.5.2. Scope limitations

This research is set to identify the change of IG waves in idealised conditions (e.g. one straight beach slope, smooth dike, etc.). Although the input conditions are taken from field sites, the assessment performed here is purely numerical modelling.

For this modelling, the 1D version of SWASH will be used, neglecting the longshore processes.

1.6. Report structure

The flow of the research is discussed in this section.

In chapter 1, an overview is given to identify the research objective and research questions. Some general themes are mentioned, only to set a background for the next chapters.

Before the research plan can be made, a thorough study of the literature will be made in chapter 2. This study focuses on IG waves and coastal wetlands and also investigates the current state of knowledge.

When the background is understood sufficiently, a plan and methodology will be suggested in chapter 3, together with a sensitivity study and discussion about the calibration of the numerical model SWASH.

This is needed before doing the modelling scenarios in chapter 4. In the same chapter, the results will be analysed and discussed, together with the strengths and weaknesses of the project and will end in a conclusion in chapter 5.

2. Literature review

The literature review of this research consists of three main parts:

1. Wave theory and IG waves;
2. Vegetated foreshores; and
3. SWASH.

They will now be discussed briefly in that order, mainly to identify the main equations and principles, and the research done by past studies.

2.1. Wave theory

It is assumed that the reader of this work has a basic understanding about wave theory and wave action. The key principles needed are briefly explained below.

An ideal, linear wave, following the Airy theory (Airy, 1845). It describes the surface elevation as a function of time and space and follows a sine form. It can be described as:

$$\eta(x,t) = \frac{H}{2}\sin\left(\frac{2\pi}{T}t - \frac{2\pi}{L}x\right) = a\sin(\omega t - kx) \qquad (2.1)$$

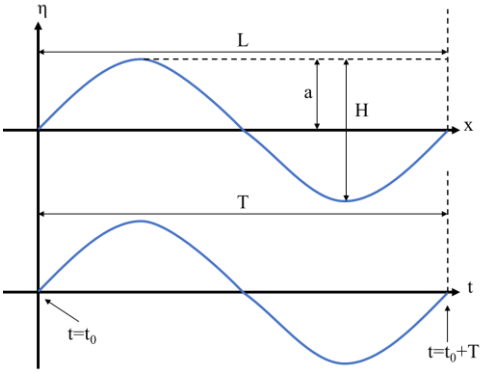

Where: η(x,t) = surface elevation [m]

H = wave height [m]

T = wave period [s]

L = wave length [m]

a = amplitude [m]

ω = radial frequency [1/s]

k = wave number [1/m]

Figure 2. Airy linear wave theory

The wave length can be determined from the wave period, using the depth h and the following equation:

$$L = \frac{gT^2}{2\pi}\tanh kh \qquad (2.2)$$

This is an iterative formula, however, there are approximations for deep and shallow water. This is defined as the ration between the water depth h and the wave length L. Where h/L < 1/20, the situation is considered as deep water, and where h/L > 1/2, it is considered as shallow water. For these two situations, the formulas are simplified as:

Deep water	Shallow water
$L = \frac{gT^2}{2\pi}$	$L = \sqrt{gh}\cdot T$

(2.3)

A wave travels at a certain speed, or wave celerity c. Using the distinction between deep and shallow water wave lengths, the celerities can be determined too:

$$\underline{\text{Deep water}} \qquad \underline{\text{Shallow water}}$$
$$c = \frac{L}{T} = \frac{gT}{2\pi} \qquad c = \frac{L}{T} = \sqrt{gh} \tag{2.4}$$

2.2. Wave mechanics

Following are some of the relevant wave mechanics, needed for this research.

2.2.1. Shoaling and refraction

When ocean waves enter coastal waters, they will be affected by the limited depth. The bottom will slow down the wave, and consequently the wave length. Because of the principle of 'conservation of energy', the amplitude of the given wave will increase. This is called shoaling. When the waves travel towards the coast, the (oblique) wave crests will bend towards the coastline to ideally normal incidence. This is called refraction (Holthuijsen, 2007).

2.2.2. Wave breaking

Wave breaking happens mainly because of two reasons: depth-induced breaking and steepness-induced breaking. Virtually, the shoaling principle could build up the amplitude until infinity, however there is a physical limit. Steepness-induced breaking assumes the wave crest will become too high and will eventually unstable. The steepness-limit is given to be H/L=1/7, where H is the wave height and L is the wave length. For depth-induced breaking, a physical limit of H/d=0.78 is given, where H is the wave height and d is the local water depth (Le Méhauté, 1969).

The bed slope also influences the breaking. Four types of breaking waves are identified, following the Iribarren number or surf similarity parameter. With a high Iribarren number (ξ_0>3.3), the breaker type will be a surging or collapsing wave. Here, the bottom is the dominant influence. A low Iribarren number (ξ_0<0.5) indicates a spilling wave. Here, the steepness of the wave will be the dominant reason for breaking. In between ($0.5 < \xi_0 < 3.3$) there is the plunging wave.

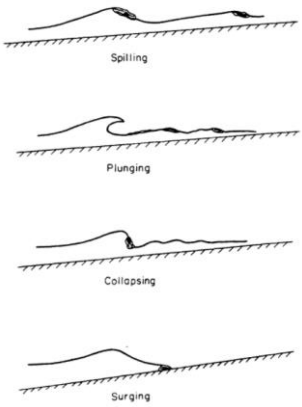

Figure 3. Breaker types. Image from (Sorensen, 2013)

$$\xi_0 = \frac{\tan\alpha}{\sqrt{H_0/L_0}} \tag{2.5}$$

Where: ξ_0 = Iribarren number [-]

α = sea bed slope

H_0 = deep water wave height [m]

L_0 = deep water wave length [m]

2.3. Infragravity waves

A unique kind of waves, and a focus in this work, are infragravity (IG) waves, a phenomenon first reported in 1949 (Munk, 1949). These waves cannot be explained without their counterpart: gravity waves. IG waves are surface ocean waves with frequencies below those of wind-generated waves (Bertin *et al.*, 2018), usually chosen to be around 0.004-0.04Hz. A lower frequency corresponds to a longer

period, therefore, IG waves are often referred to as ‘long waves’, while wind waves can be seen as ‘short waves’. A short overview about the mechanics of these IG waves follows:

2.3.1. Generation

As the wind blows over the ocean, it will generate waves. These waves are called wind waves, or sometimes gravity waves (because gravity is the restoring force that dampens these waves). These are usually formed in a storm front, where the wave field is random and moves in all directions. These waves will move out of the random storm field. These residual waves are defined as ‘swell waves’ and will move following the dispersion relation. Briefly said, different waves will travel at different speeds, depending on their frequency (Whitham, 1974).

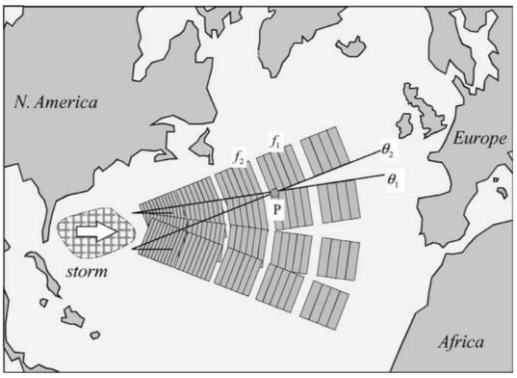

Dispersion relation:

$$\omega^2 = gk\tanh(kh) \qquad (2.6)$$

Where: ω = radial frequency [1/s]

g = gravitational acceleration [m/s²]

k = wave number [1/m]

h = water depth [m]

Figure 4. Dispersion relation for oceanic waves. Image from (Holthuijsen, 2007)

Swell waves will usually propagate towards the shore, towards shallow water. Following the linear wave theory and the dispersion relation, in deep water, $tanh(kh) \approx 1$, making the individual velocity $c = \frac{gT}{2\pi}$, in other words; in deep water environments, the wave velocity depends solely on the frequency. Waves that have frequencies close to each other, as seen in Figure 5, will have a tendency to group. This is called a bichromatic wave field. They will move in more organised patterns and form one residual wave, sometimes strengthening or weakening each other.

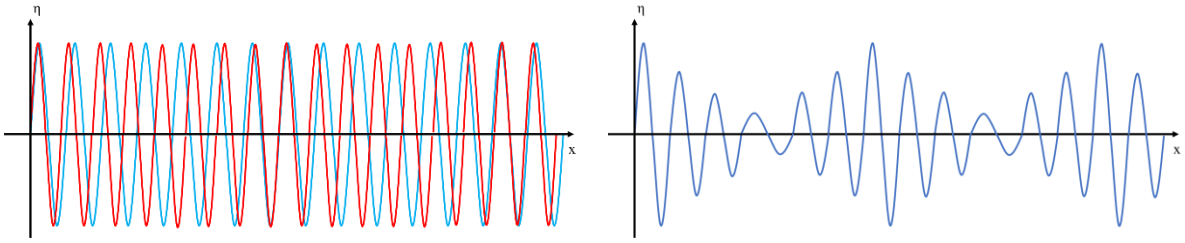

Figure 5. Bichromatic wave field where (left) the blue wave has a slighty larger period than the red wave and (right) the one residual wave is represented.

When the incident gravity wave groups are propagating towards the shore, they will lose energy, and this coincides with a change in momentum, a depth-averaged momentum flux. This is defined as ‘radiation stress’ (Longuet-Higgins and Stewart, 1962, 1964). Through nonlinear interaction, or second-order Stokes interaction, this causes a forced local set-up (or set-down) in the sea level and tends to generate a secondary wave, with a length similar to the whole wave group length, but with a very small amplitude. This secondary wave is the ‘IG wave’. As these waves are generated and even forced by the wave group of the shorter waves, they will travel together at the group speed, rather than the individual phase speed, making them a ‘bound wave’. This is shown in the next figure. The secondary IG wave is 180° out of phase with the wave group length. This means that there will be a set-down of the water

level when the wave group is at its maximum amplitude and a set-up at the smaller amplitude waves (Van Dongeren, Reniers and Battjes, 2003; Bertin *et al.*, 2018).

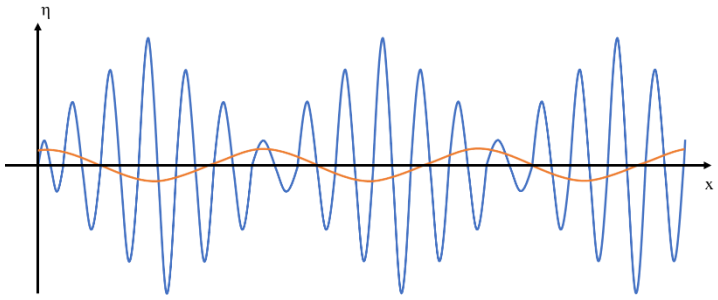

Figure 6. Representation of wave grouping. Groups of deep water gravity waves (blue) and the bound IG wave (orange). The waves are 180° out of phase. Image modified from (Longuet-Higgins and Stewart, 1964).

The equation for the surface elevation of the second-order bound wave is given to be (Longuet-Higgins and Stewart, 1962):

$$\eta(x,t) = -\frac{1}{\rho}\left[\frac{S_{xx}(x,t)}{(gh - c_g^2)}\right] \tag{2.7}$$

Where: $\eta(x,t)$ = surface elevation [m]

ρ = water density [kg/m³]

$S_{xx}(x,t)$ = radiation shear stress in cross shore direction [N/m²]

g = gravitational acceleration [m/s²]

h = water depth [m]

c_g = group velocity [m/s]

This wave grouping can be seen as one of two main generation mechanisms of IG waves. The other is defined as *moving breakpoint* and happens during the shoaling, and more importantly breaking of the gravity waves. Short waves are susceptible to breakpoint forcing (a moving breakpoint). Waves with different heights will break at different locations, resulting in a time-variation of the radiation stress, and a time-varying set-up as a consequence. This is the second generation mechanism.

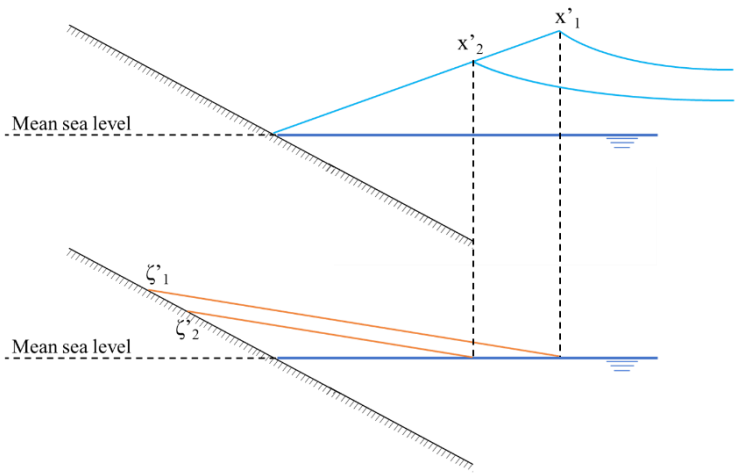

Figure 7. Schematic representation of breakpoint forcing. The top image represents the breaking gravity waves, the bottom image depicts the set-up as a result from breaking. Image modified from (Symonds, Huntley and Bowen, 1982).

2.3.2. Growth of IG waves

During the shoaling process of gravity waves, the long bound will shoal too. When the gravity waves break, their bound long wave is released and would propagate towards the coastline (or even towards the sea), and the extra set-up due to moving breakpoint is generated. Higher waves will generally break further offshore, thus the two generation mechanisms for the IG wave happen sooner and there is more time and space for the IG wave to develop. (Symonds, Huntley and Bowen, 1982). An attempt to predict the amplitude growth of the IG wave has been made. This shoaling of incoming long waves is determined to be a function of the normalized bed slope parameter (Battjes *et al.*, 2004):

$$\beta_s = \frac{\alpha}{\omega}\sqrt{\frac{g}{h}} \tag{2.8}$$

Where: β_s = normalized bed slope parameter [-]

α = bed slope [-]

ω = radial frequency of the IG frequency band [1/s]

g = gravitational acceleration [m/s²]

h = water depth [m]

The amplitude of the IG wave should lie between Green's law for conservative shoaling (increase proportional to $h^{-1/4}$) and the shallow-water equilibrium solution (increase proportional to $h^{-5/2}$), where h equals the water depth (Van Dongeren *et al.*, 2007). This formula basically classifies incoming waves as a function of the bed slope parameters (h and h_x) and their frequency. Note that the radial frequency is taken for the This is similar to the earlier mentioned Iribarren number ξ_0 where the breakers are classified following steepness and bed slope. Here, $\beta_s<0.06$ means there is enough room for an amplitude growth, similar to high-frequency waves and closer to the shallow-water equilibrium solution ($h^{-5/2}$). A value of $\beta_s>0.30$ indicates a weak amplitude growth, closer to Green's law ($h^{-1/4}$).

It is important to know how large the set-up due to IG waves is in reality, because this increases the mean-water level (MWL) and

2.3.3. Energy transformation

As it has been stated, IG waves will either break in shallow water or propagate towards the shoreline and cause an increase in run-up. The energy of the IG waves however can do either one of two things: dissipate or reflect (Bertin *et al.*, 2018). A difference can be made between steep and gently sloping beaches. It has been noticed that on steep beaches, which coincides with a high value of both the bed slope parameter β_s and Iribarren number ξ_0, the IG waves will interact with the short waves from the group and energy (at low frequencies) will dissipate after breaking into a wide range of higher frequencies, fewer on the IG frequencies (de Bakker, Tissier and Ruessink, 2015). When the slope is gentle however (β_s and ξ_0 are small) the IG wave will interact more with the other IG waves, rather than the short gravity waves. This could cause the IG waves to steepen and break following the steepness limit for breaking, making a larger dissipation of the IG frequency energy.

Although IG waves were previously not considered to have a serious impact, they can become rather important in the breaker zone of the coast. Waves are depth-limited, so when they enter the surf zone, they will likely start shoaling and break. Most of their wave energy is then dissipated. However, not all energy is lost in the wave breaking. Some is transferred to the IG wave. In shallow water, through the dispersion relationship, the individual velocity of a wave shifts to $c = \sqrt{gh}$, in other words, only dependant on the water depth. However, the IG waves start lagging behind on the wave group. It is this

shift in phase difference that allows the wave group to transfer energy towards the long waves (List, 1992; Masselink, 1995). As IG waves have smaller amplitudes, they don't break together with their wave group, and through the energy transfer, they can propagate towards the shoreline. This phase lag was observed and confirmed by field data (Masselink, 1995), but there is still discussion about how this phenomenon actually works.

2.3.4. Longshore effects

For this whole work, the assumption of only cross-shore effects is made. That is however a big simplification. For obliquely incoming waves, wave refraction is larger. Furthermore, the refraction of free IG waves is larger than IG waves still bound to their wave group. In some cases, when the angle of incidence is large enough, the IG wave could become trapped to the shoreline. This could lead to resonance, where even the incoming short waves transfer energy to the coastally trapped IG waves. These are defined as *edge waves* (Reniers *et al.*, 2002; Bertin *et al.*, 2018). The edge waves formed by oblique waves are usually standing in the cross-shore direction, but progressive. They have been shown to vary depending on the slope steepness, and don't necessarily in the IG frequency band (Guza and Davis, 1974). Assuming only cross-shore effects will probably result in an overestimate of the IG wave, so an overestimation of the IG dominance.

2.4. Shallow foreshores

The foreshore has multiple definitions. One of those is the part in front of the dike, with a slope ranging from 1:10 to horizontal (Altomare *et al.*, 2016), or simply the area of the shore between mean high water and mean low water (CUR, CIRIA and CETMEF, 2007).

In this research, the emphasis lies on shallow foreshores. A rule of thumb is when waves break due to depth rather than steepness, the foreshore can be considered shallow or very shallow. Up to date, there is no universal definition of what the limits of a shallow foreshore or a very shallow foreshore are (Altomare *et al.*, 2016). One attempt has been made, which is illustrated in Figure 8. The theory compares the offshore wave height H_{m0} with the water depth at the toe h_{toe} (van Gent, 1999). When this ration of H_{m0}/h_{toe} lies between 0.75 and 1.50, the foreshore is considered to be shallow. Is it higher than 3.0, it is considered very shallow.

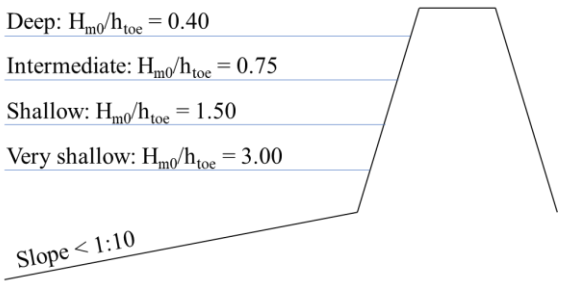

Figure 8.Foreshore classification. Adapted from (Altomare *et al.*, 2016).

Adding this to the Iribarren number (equation 2.5) and the normalized bed slope parameter (equation 2.8), a shallow or very shallow foreshore is assumed to have low values of both parameters. This could indicate that waves will start breaking further offshore, in comparison to intermediate or deep foreshores. This would mean the bound IG wave gets released earlier and can run-up higher, creating more IG energy. This is confirmed by other researches, where in a mildly-sloping beach, the IG energy was noticed to be more developed, and on a steep-sloping beach, the swell-waves were dominant (de Bakker, Tissier and Ruessink, 2015).

2.5. Vegetation

The studies about the effect of vegetation on IG waves are very limited. There is no apparent paper in a lab study, but in some cases, there is mention of IG waves for a study with vegetation present (Vuik *et al.*, 2016). An analogy can be drawn between the effect of vegetation and coral reefs, as both reefs and plants have increase bottom friction, drag and basically function as an obstacle for the waves to propagate undisturbed. Therefore a recent set of papers of IG waves and coral reefs can be used as a red thread in examining this (Van Dongeren *et al.*, 2013; Ma *et al.*, 2014; Su, Ma and Hsu, 2015; Su and Ma, 2018). Before going into the effects of vegetation on IG waves, a short overview of the general effect of vegetation on wave propagation is given.

It is known and proven that vegetation is beneficial and cause wave damping and dissipation of the wave energy. In general, four different kinds of natural habitats are identified (Narayan *et al.*, 2016). The global distributions per habitat are given in Figure 9:

- Reefs;
- Mangroves
- Sea grass;
- Salt marshes.

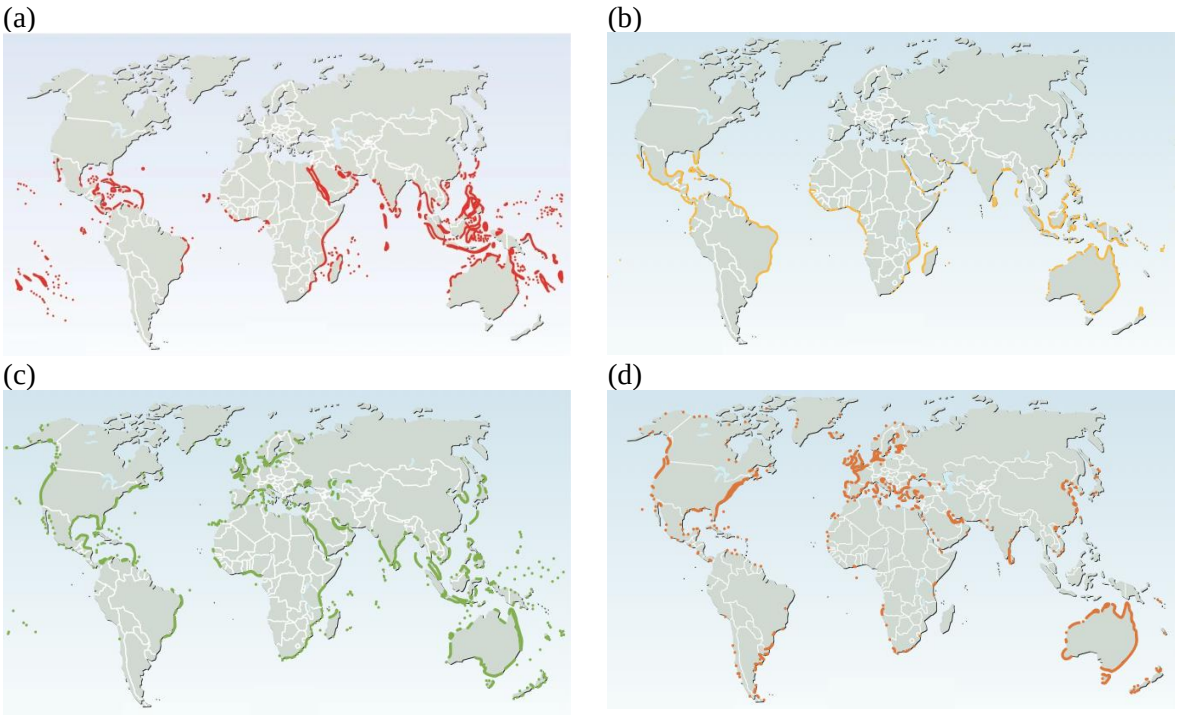

Figure 9. Global distribution of habitats. (a) Reefs (b) Mangroves (c) Seagrass and (d) Salt marshes (Image adapted from (UNEP, 2014; UNEP-WCMC, 2017)*)*

In case of the test sites selected for this research, reefs and mangroves are unlikely, so the focus here will be on the effect of seagrass and salt marshes on the wave dissipation. Out of all the wave actions and processes, seagrass will have an effect on shoaling and the bottom friction and a salt marsh is effective in reducing wave height (by breaking), reducing run-up and increasing bottom friction and the drag coefficient. These effects of vegetation on these specific wave mechanics are now looked at separately:

2.5.1. Wave propagation

The effects of the vegetation on the waves depend on several factors. First of all, there are vegetation properties (stem thickness, vegetation density and stem height), second there are the hydrodynamic characteristics (wave height, wave period, water depth) and finally, there is the bottom topography (Mendez and Losada, 2004).

As a wave propagates in a foreshore, it will lose energy. This has three main reasons: depth-induced wave breaking, bottom friction, and in some cases vegetation (or vegetation drag). Multiple studies have proven a direct relation between vegetation and energy dissipation (Mendez and Losada, 2004; Dean and Bender, 2006; Vuik *et al.*, 2016; Narayan *et al.*, 2017), all showing that a higher vegetation density results in higher dissipation. One of these researches has put this into an equation (Mendez and Losada, 2004):

$$\varepsilon_v = \frac{2}{3\pi}\rho C_D b_v N \left(\frac{kg}{2\omega}\right)^3 \frac{\sinh^3 k\alpha h + 3\sinh k\alpha h}{3k\cosh^3 kh} H^3 \tag{2.9}$$

Where the dissipation depends on several wave characteristics (wave number k, angular frequency ω) and environmental characteristics (water depth h), the dissipation also depends on multiple vegetation parameters, such as the drag coefficient C_D, the stem diameter b_v, the vegetation density N and the relative vegetation height α. Some studies have discussed that the vegetation height is important, and that submerged vegetation dissipates less energy than emerged vegetation (Smith, Bryant and Wamsley, 2016) and that there is a huge seasonal difference (Paul and Amos, 2011).

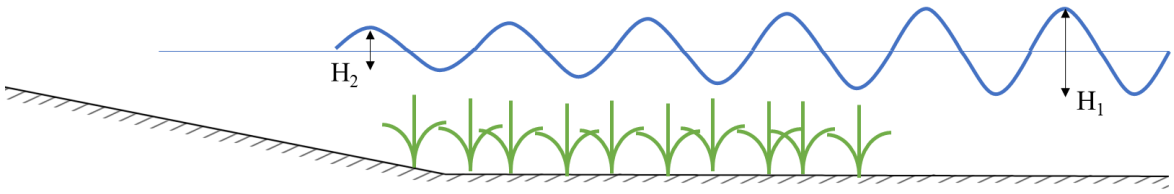

Figure 10. Wave height reduction due to vegetation.

2.5.2. Drag coefficient

Wave propagation will be hindered by the presence of 'longer' plants in the water. For example stems and branches will increase the drag coefficient of waves and will dissipate their energy (Dalrymple *et al.*, 1984), this is identified as the drag coefficient C_D.

Modelling the drag coefficient in a software model is complex and is not exact. Plants will have a strange form and measuring the individual measurements of every stem is an impossible job. Therefore, model will assume the plant stems to be of a cylindrical form. This gives good results in some cases, when the plants have not much freedom to move (Mendez and Losada, 2004). When their stiffness is low or their buoyancy is high, the problem becomes more complex.

There exist several different ways of formulating the drag coefficient. Most equations look similar, with only some parameters different. What they have in common is that they are all related to either the Reynolds number Re or the Keulegan-Carpenter number KC. It was shown that the C_D is slightly better when calculated with the Re number, although only slightly (Anderson and Smith, 2013). The 'obstacles' in shallow water created by the stems will increase turbulent flow. However, estimates in simulations are often not accurate, as they are often modelled from a field data set, and not from the forces on the plants; or the models only assume the drag coefficient to be a source of wave energy

dissipation by vegetation (Hu *et al.*, 2014). Some equations are given below. First, the Reynolds number for plants is calculated as:

$$Re = \frac{u_{max} b_v}{\nu} \tag{2.10}$$

Where: u_{max} = maximum horizontal particle velocity [m/s]

b_v = plant stem diameter [m]

ν = kinematic viscosity of water, here $\nu = 10^{-6}$ m²/s

While the KC-number is given by:

$$KC = \frac{u_{max} T}{b_v} \tag{2.11}$$

Where: u_{max} = maximum horizontal particle velocity [m/s]

T = wave period [s]

b_v = plant stem diameter [m]

One possible relation for the drag coefficient and the Reynolds number is given by (Méndez, Losada and Losada, 1999) and modified by (Hu *et al.*, 2014):

$$C_D = 1.04 + \left(\frac{730}{Re}\right)^{1.37} \qquad for\ 300 < Re < 4700 \tag{2.12}$$

Where: C_D = drag coefficient [-]

Re = Reynolds number [-]

Another version of this equation was determined from a sensitivity analysis of the drag coefficient (Anderson and Smith, 2013):

$$C_D = 0.76 + \left(\frac{744}{Re}\right)^{1.27} \qquad for\ 500 < Re < 2300 \tag{2.13}$$

A third equation is given by (Jadhav and Chen, 2012):

$$C_D = 2 \cdot \left(0.18 + \frac{1300}{Re}\right) \qquad for\ 600 < Re < 3200 \tag{2.14}$$

Also relations between C_D and the KC number are used, but are less frequently used than relating the drag coefficient to Re. An example of a KC-related equation is given here (Peruzzo *et al.*, 2018):

$$C_D = 6.5 \cdot \left(\frac{1}{KC}\right)^{0.64} \tag{2.15}$$

This to only name a few. What is noticeable is that the drag coefficient increases with a decreasing Reynolds number. There is no current way to select the best equation. A suggestion is a value of 1.0 for the maximal force on the stems. However, the stems are not rigid cylinders as often portrayed in models but have a tendency to bend and move with the waves. Therefore, based on previous literature, a drag coefficient ranged from 0.4 to 0.6 is a well estimated guess, to approximate reality (Vuik *et al.*, 2016; Keefer *et al.*, 2017). What is important to note, is that only one vegetation parameter is shown in the drag coefficient, which is the stem diameter. This means that this coefficient doesn't distinguish emerged and submerged vegetation, or takes the plant density into account.

2.5.3. Depth-induced breaking

As mentioned before, the maximum wave height in shallow water depends largely on the water depth. Several types of vegetation may almost 'raise the sea floor', so waves would shoal and break earlier in the surf zone. Here, the same conclusion can be made as with the beach slope, the depth-induced breaking depends on the ratio between the offshore wave height and the water depth at the toe. When this ratio is low (<0.15), or in deep foreshores, depth-induced breaking is negligible and wave attenuation by vegetation can be considered small. When this ratio is higher, or intermediate foreshores, the effect of vegetation on depth-induced breaking becomes more significant, and can dissipate up to 50% of the wave height reduction (Vuik *et al.*, 2016). However, when this ratio becomes very high, in other words shallow and very shallow foreshores, depth-induced wave breaking becomes largest, but the contribution of vegetation becomes smaller, as the vegetation contributes more to the dissipation of wave energy, rather than breaking, and a distinct breaker zone is absent.

2.6. SWASH

There are several models that are capable to simulate IG waves, such as XBeach (Hewageegana *et al.*, 2017; Lashley *et al.*, 2018), but in this study, the software SWASH is chosen. This choice mainly goes out from the multiple vertical layers, which could be a large advantage in correctly simulating wave dispersion and getting the IG waves more exact.

The prediction for transformation of surface waves will be done with this model, SWASH (Simulation WAves till SHore). It is a numerical model for simulating non-hydrostatic, free-surface rotational flows in one, two or three dimensions (The SWASH team, 2017). Some aspects of SWASH are mentioned here:

- Non-hydrostatic: The momentum equations make some assumptions. One of those is for the vertical momentum equation, that the pressure is hydrostatic, or in other words that the fluid is at rest. Non-hydrostatic pressure models assume a moving fluid (LaCasce, 2008).
- Phase-resolving: a phase-resolving software will simulate every wave individually. This is necessary to simulate IG waves.
- Non-linear: The energy transfer from the wave groups to the IG waves is considered non-linear, therefore a system is needed that can simulate this.
- Free-surface flow: SWASH simulates the changes of the wave-form, so the water surface, or free surface.
- Rotational flow: Rotational flow means that water particles are assumed to circle around, as well as spin around their own axis. Again, this is moving away from linear wave theory.

The governing equations behind the model are the nonlinear shallow water equations including non-hydrostatic pressure and some transport equations (Zijlema, Stelling and Smit, 2011). They are given below:

$$\frac{\delta\zeta}{\delta t} + \frac{\delta hu}{\delta x} + \frac{\delta hv}{\delta y} = 0 \tag{2.16}$$

$$\frac{\delta u}{\delta t} + u\frac{\delta u}{\delta x} + v\frac{\delta u}{\delta y} + g\frac{\delta\zeta}{\delta x} + \frac{1}{h}\int_{-d}^{\zeta}\frac{\delta q}{\delta x}dz + c_f\frac{u\sqrt{u^2+v^2}}{h} = \frac{1}{h}\left(\frac{\delta h\tau_{xx}}{\delta x} + \frac{\delta h\tau_{xy}}{\delta y}\right) \tag{2.17}$$

$$\frac{\delta v}{\delta t} + u\frac{\delta v}{\delta x} + v\frac{\delta v}{\delta y} + g\frac{\delta\zeta}{\delta y} + \frac{1}{h}\int_{-d}^{\zeta}\frac{\delta q}{\delta y}dz + c_f\frac{v\sqrt{u^2+v^2}}{h} = \frac{1}{h}\left(\frac{\delta h\tau_{yx}}{\delta x} + \frac{\delta h\tau_{yy}}{\delta y}\right) \tag{2.18}$$

In these equations, ζ(x, y, t) represents the water elevation, u(x, y, t) and v(x, y, t) are the depth-averaged flow velocities in respectively x and y direction, q(x, y, z, t) is the non-hydrostatic pressure, c_f represents a friction coefficient and finally, τ_{xx}, τ_{xy}, τ_{yx} and τ_{yy} are the turbulent stress terms. Furthermore, the integral of the non-hydrostatic pressure is expressed as:

$$\int_{-d}^{\zeta} \frac{\delta q}{\delta x} dz = \frac{1}{2} h \frac{\delta q_b}{\delta x} + \frac{1}{2} q_b \frac{\delta(\zeta - d)}{\delta x} \tag{2.19}$$

An important part of SWASH, which distinguishes it from other software, is the option to add multiple vertical layers. With this option, the wave celerity will be determined different times, per vertical layer. Due to the dispersion relation, the wave speed depends on the water depth in shallow water. Incorporating different layers, means the wave celerity can be calculated varying over the depth, which would return with a more accurate representation of the reality. The model improves its frequency dispersion by increasing the number of vertical layers (The SWASH team, 2017).

It is also possible to add vegetation into SWASH. This is done by using the stem height, diameter, plant density and drag coefficient as input for the model. In SWASH, within the vegetation canopy, it is assumed that all energy of the mean flow is converted to turbulent energy due to the plant drag. This vegetation-induced turbulence mixing is resolved using the k−ε model for turbulence. Without going into too much detail, this is a model with two equations, solving for the turbulent kinetic energy k(x, t) and the rate of dissipation of turbulent energy ε(x, t) (Scott-Pomerantz, 2004).

2.7. State of current research

There has already been some research in the field of IG waves. This work will attempt to be an extension of previous works. A short overview of what has been done follows:

IG have come a long way since their discovery in 1949, as can be seen in the increasing rate of number of publications about the topic in Figure 11. There were multiple experiments in both labs as in the field, and the development of software has come further, where IG waves can now be simulated in phase-resolving software like SWASH. Recent studies have been more and more around case studies (Bertin and Olabarrieta, 2016; Inch *et al.*, 2017; Su and Ma, 2018). A topic that is actively researched is the effect of the beach slope on the IG wave (de Bakker, Tissier and Ruessink, 2015; Fiedler *et al.*, 2018; Gomes da Silva *et al.*, 2018). Also the effect of IG waves on the run-up of a beach is deemed more important now (Roelvink *et al.*, 2017; Lashley *et al.*, 2018)

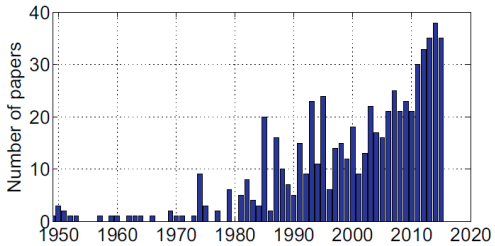

Figure 11. Number of papers with IG wave or surf beat in the title. Image from (Bertin *et al.*, 2018).

Research papers assessing the propagation and mechanics of IG waves in a vegetated environment, such as salt marches, are very scarce (Vuik *et al.*, 2016), none deals directly with this topic. There have however been studies about the effects of mangroves (Hewageegana *et al.*, 2017) and coral reefs on IG waves (Van Dongeren *et al.*, 2013). Mainly the effects of coral reefs on IG waves have been documented recently (Roeber and Bricker, 2015; Su, Ma and Hsu, 2015; Su and Ma, 2018). As the effects of corals and vegetation can be considered similar, they can be an inspiration to assess the effects of vegetation from e.g. salt marshes on IG waves.

3. Methodology

The ultimate goal of this project is to successfully simulate and analyse IG waves in different conditions and determine where IG waves are the most dominant. Here, some more explanation is provided into how this will be accomplished. This to give insight into the research and make it trustworthy and give the ability to reproduce it. To accomplish this with the numerical model SWASH, the preparation work can be separated in some steps.

1. Sensitivity analysis of model parameters;
2. Calibration of the model;
3. Validation of the model;
4. Selecting input scenarios;

To start, some more info is given about the validation of the model.

3.1. Validation method

Before any of the simulations can be done, the model and input file need to be validated. To do this, the observed results from a lab experiment from Flanders Hydraulics, Belgium (Altomare *et al.*, 2016) are compared to the results from several SWASH simulation with the same input. The comparison is done using several validation methods, based on previous researches (Roelvink *et al.*, 2009; Lashley *et al.*, 2018):

1. Root-mean-square error ($RMSE_\Psi$):

$$RMSE_\Psi = \sqrt{\frac{1}{n}\sum_{i=1}^{N}(\Psi^i{}_{SWASH} - \Psi^i{}_{observed})^2} \tag{3.1}$$

The RMSE measures the difference between the SWASH and the observed value and is a commonly used measuring tool.

2. Scatter Index (SCI_Ψ):

$$SCI_\Psi = \frac{\sqrt{\frac{1}{n}\sum_{i=1}^{N}(\Psi^i{}_{SWASH} - \Psi^i{}_{observed})^2}}{\frac{1}{n}\sum_{i=1}^{N}\Psi^i{}_{observed}} \tag{3.2}$$

The SCI represents the RMSE, normalized over the observed mean. This value is considered ‘perfect’ for a 0.0 value. The ideal target of this SCI is less than 0.10 (Roelvink *et al.*, 2009), but for other studies with high detailed wave models, a SCI less than 0.30 was found acceptable (Mazarakis *et al.*, 2012; Mentaschi *et al.*, 2013).

3. Relative bias ($Rel.bias_\Psi$):

$$Rel.bias_\Psi = \frac{\sum_{i=1}^{N}(\Psi^i{}_{SWASH} - \Psi^i{}_{observed})}{\sum_{i=1}^{N}\Psi^i{}_{observed}} \tag{3.3}$$

This parameter is similar to the SCI, as it is normalised in the same way. However, where the SCI is based on the RMSE, the Rel.bias also accounts for the over -or underpredicting of a model. Equal to the SCI, the Rel.bias is considered ‘perfect’ for 0.0 and the same target values are tried to be obtained.

Based on previous works, the SCI and the Rel.bias can be represented in the following figure (Lashley *et al.*, 2018). This illustrated that everything within the border of the red line is considered acceptable, and points within the green border represent an ideal performance of the model.

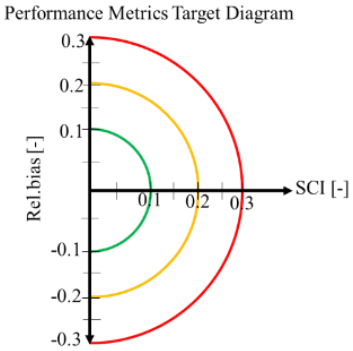

Figure 12. Performance target diagram. Within the green line means both a SCI and Rel.bias of under 10%, within the orange line means less than 20%, and within the red line less than 30%.

While conducting the sensitivity analysis on the input parameters, this target diagram will be used to analyse the wave heights H_{m0} at three different locations in the wave flume and compare the observed and simulated values.

Furthermore, the water elevation η will be compared by taking the average values of the water-level time-series.

3.2. Infragravity analysis

The effects of IG waves should be quantified, this means that the IG waves should be identified correctly. A normative way to separate IG waves from gravity waves, is to separate them by frequency. The values of 0.004-0.04Hz is often chosen to represent IG waves as a static approach. Here, a more dynamic representation is selected, to limit IG waves between 0.005Hz and half the peak frequency f_p (Lashley *et al.*, 2018).

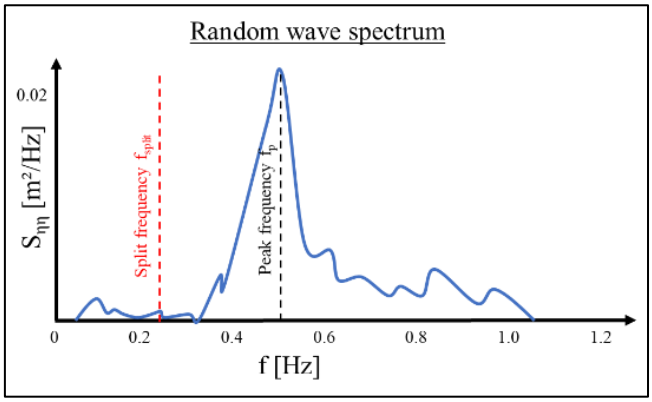

Figure 13. Visualisation of a wave spectrum computed from a time series.

The wave height H_{m0} can also be separated into a low frequency wave height (for IG waves) and a high frequency one (for gravity waves).

$$H_{m0,LF} = 4\sqrt{\int_{0.005}^{f_{limit}} S_{\eta\eta}\,df} \tag{3.4}$$

And;

$$H_{m0,HF} = 4\sqrt{\int_{f_{limit}}^{\infty} S_{\eta\eta} df} \tag{3.5}$$

These two wave heights are related to one another with the following equation:

$$H_{m0,Total} = \sqrt{H_{m0,LF}^2 + H_{m0,HF}^2} \tag{3.6}$$

One of the questions in this research is how to identify the IG waves, and how to assess the dominance. Using these two wave heights, the Infragravity coefficient (IGC) is computed to quantify the IG waves. If the IGC is larger than 1, the IG waves dominate, if smaller than 1, gravity waves dominate. This coefficient can be determined anywhere over the slope, but for this research the IGC will mainly be determined at the dike toe.

$$IGC = \frac{H_{m0,LF}}{H_{m0,HF}} \tag{3.7}$$

The coefficient might be good to select whether IG waves are dominant or not, but it is a relative representation and does not show the evolution of the total wave height (for instance wave height reduction by vegetation is not represented in the IGC). Therefore, a second assessment coefficient is introduced, where the wave height at the toe of the dike is represented relative to the offshore wave height:

$$H_{m0,rel.} = \frac{H_{m0,,toe}}{H_{m0,offshore}} \tag{3.8}$$

This last mentioned coefficient is especially useful to compare the wave reduction with and without vegetation. It can also be modified, changing $H_{m0,\ toe}$ into either $H_{m0,\ LF,\ toe}$ or $H_{m0,\ HF,\ toe}$ to investigate the two different wave heights separately.

3.3. Lab experiment

The lab test was done in Flanders Hydraulics, Belgium. An idealised profile was made to simulate a beach and a dike at the Belgian coast (Altomare *et al.*, 2016). The wave flume was equipped with a wave maker on one side and four different dikes on the other side, at 46m from the wave maker. The wave maker was used to create a JONSWAP wave spectrum (γ=3.3). Over the whole length of the flume, there were some sensors that measure the surface elevation, using resistance-type wave gauges. This whole test was done on a 1:25 scale. There was no vegetation present in the experiment.

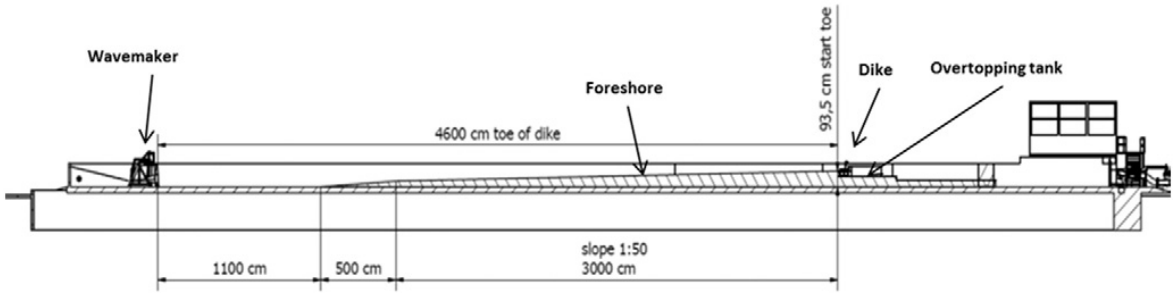

Figure 14. Model setup (Altomare *et al.*, 2016).

The locations of the different sensors, as well as the bathymetry of the wave flume is given in Figure 15:

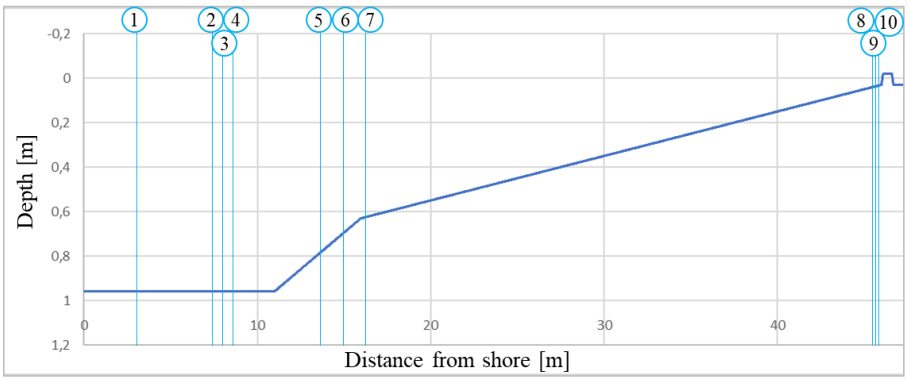

Sensor	Distance from wave maker [m]
1	3.415
2	7.94
3	8.38
4	9.00
5	13.94
6	14.84
7	15.84
8	45.54
9	45.79
10	45.96

Figure 15. Bathymetry and location of the sensors.

As can be noticed in the previous figure, the bathymetry is not one straight line. First there is a kink of 1:15 slope for 5m, after which the selected slope of 1:50 starts. This is done to limit the space in the flume for the physical experiment. A rule of thumb is that the biggest wave would break at a depth h where $2H_{m0}=0.6h$ (Baldock, 2012), which here accounts for the depth at the end of the kink.

3.3.1. Input parameters

Before the simulation can be done with varying parameters, the model input file needs to be defined and assessed. This is done for the lab data. The grid size, number of layers and overall evaluation of SWASH are investigated. The input parameters for the lab experiment are given in Table 1. These are measured from actual lab measurements and will be used as comparison.

Table 1. Input parameters sensitivity analysis.

Test	H_{m0} [m]	T_P [s]
1	0.0563	2.2825
2	0.0483	2.1989
3	0.0497	2.1934
4	0.0518	2.4849
5	0.0668	2.2979
6	0.0569	2.5300
7	0.0999	2.3210
8	0.1212	2.2990
9	0.0684	2.2836
10	0.0649	2.2825
11	0.1140	2.3089

Later on, a detailed analysis of the overall performance of SWASH will be executed. Before that however, a rough analysis is done to determine the grid size and the number of layers. This can be seen in Appendix 1 and is summarized here. These input parameters are taken into the overall sensitivity analysis. The decision was made on accuracy of the wave height and wave spectrum and the optimal run time. The ultimate choice goes to a grid cell size of 100 cells per wave length, which was an average of 7.5cm. Furthermore, 2 layers was found to be more optimal than 1 layer. The accuracy of the model output did not increase significantly when moving up to 3 layers.

3.3.2. Calibrating SWASH

Using the grid size of 100 cells per wave length (or 7.5cm) and two layers, a simulation is executed using the default settings of SWASH. This is analysed in Appendix 2, and the conclusion is shown here.

The output from the simulations software is compared to measurements made in the lab experiment. In general, the first analysis shows very accurate results near the wave maker, both in low and high-frequency wave heights. However, the performance of the model near the dike shows inaccurate results, especially from the high frequency wave heights. The results for the sensor closest to the dike are shown in Figure 16. The low frequency wave heights are acceptable (SCI=0.09184, Rel.bias=-0.04827), however the results of the high frequency wave height is very off and the model underpredicts in most cases (SCI=0.29195, Rel.bias=-.013013). Because the IGC is calculated using these two, it also show very wrong results (SCI=0.25635). Note that the Rel.bias determines whether the model is under -or overpredicting, when all results are very scattered, it does not correctly represent the performance of the model on its own.

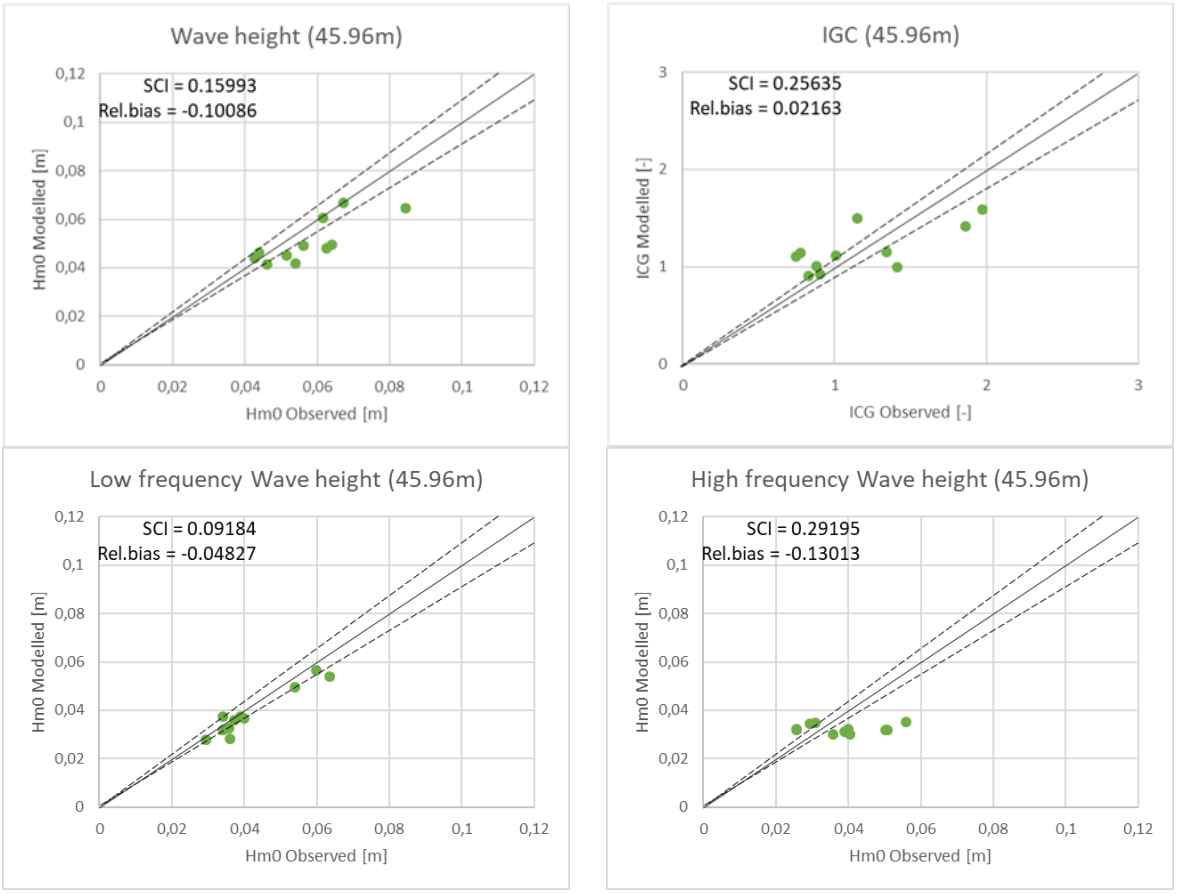

Figure 16. Performance of SWASH before calibration. Wave sensor closest to the dike. The full line is the 0 deviation line, the dotted lines are a 10% deviation.

The accuracy of the model can be increased by changing the breaker parameters α and β and SWASH and introducing the simulation to a friction coefficient.

First of all, the breaker parameter is varied. In SWASH, energy dissipation due to breaking is always taken into account, however the program makes some calculated estimations, such as the phase velocity and energy dissipation in the front of the wave train in shallow water. SWASH tracks the front of this wave train using the shallow water celerity, making sure it is never too much out of range. The default value for α is 0.6 and can be translated as the parameter at which to initiate wave breaking. The same

story holds for the breaker parameter β, which is the parameter at which to stop wave breaking. The default value for β is 0.3. Both parameters are defined as:

$$\frac{\delta\zeta}{\delta t} > \alpha\sqrt{gh} \quad and \quad \frac{\delta\zeta}{\delta t} > \beta\sqrt{gh} \tag{3.9}$$

Where ζ is the vertical speed of the free surface. From the initial runs of the model, it is concluded that the model is too dissipative. This can be helped by increasing the breaker parameters. In practise, this means that the waves would start breaking further in the wave flume. From the breaker parameter analysis in Appendix 2, the model is seen to perform a little better with a breaker parameter α of 0.9 and a breaker parameter β of 0.6, although the effect is not very large. Finally, a friction Manning coefficient is introduced, this can be seen in Appendix 2. The sensitivity analysis of the friction coefficient gives an optimal value of 0.02 $m^{-1/3}s$ as Manning coefficient for the model input.

3.3.3. Model validation

Now that all parameters are determined, a final analysis is done to validate the model. This is done by simulating all different experiments from the lab and comparing the SWASH output results with the observed values. Every time, the comparison is made at three different locations, once near the wave maker to investigate if the wave is simulated correctly, and twice near the dike to investigate if the wave breaking is simulated accurately.

For starters, the total wave heights are compared at the three locations. The performance of the model can be concluded very good when only looking at the total wave height H_{m0}, near the wave maker the performance is really well (SCI=0.02133, Rel.bias=0.01770), but also near the dike, the model and the reality are closely related (SCI=0.07721, Rel.bias=-0.06197 and SCI=0.08631 and Rel.bias=0.05168).

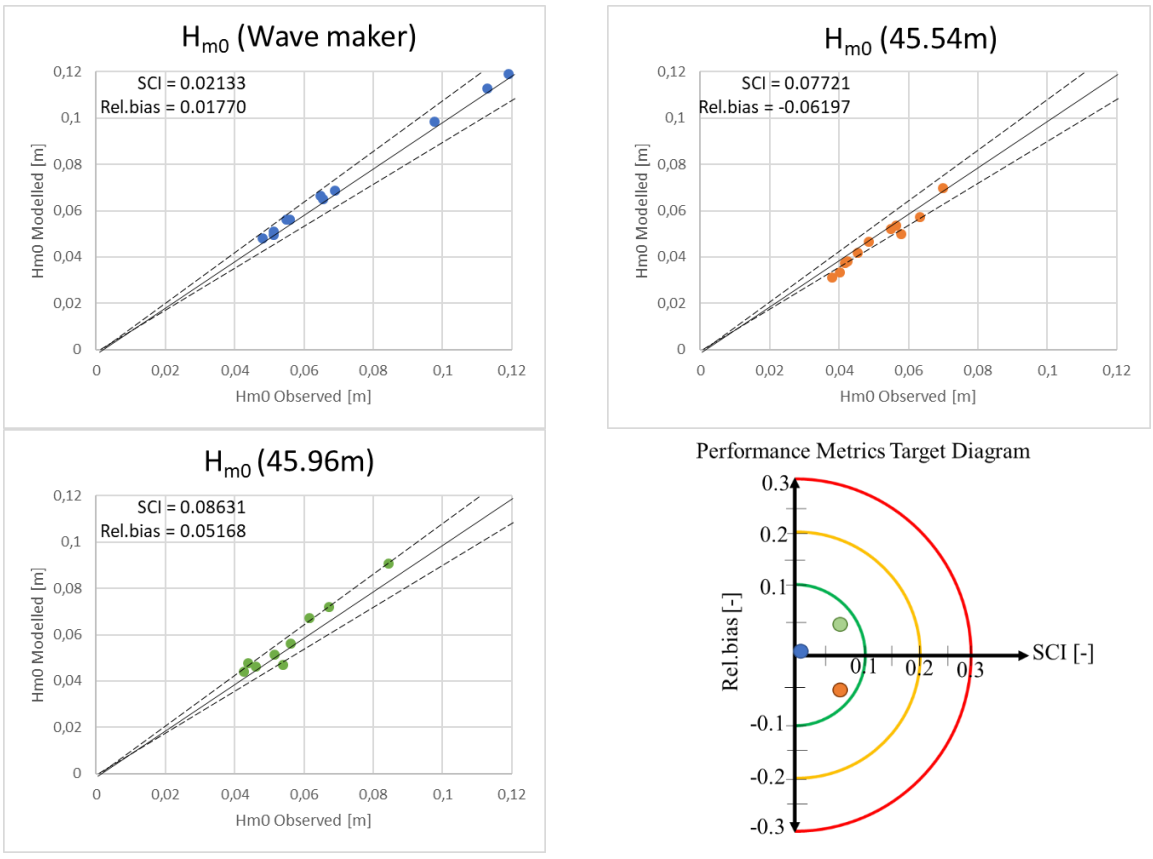

Figure 17. Model validation for H_{m0}

However, this alone is not enough. For all three locations, the wave heights are split up into their high and low frequency components. This is shown in Figure 18. As before, the accuracy at the wave maker is optimal. The SCI for the low frequency wave heights is a little higher (SCI-0.11380) but this can be explained by the fact that the low frequency component is so small that every deviation results in a high error. Overall, the SWASH results are very closely related to the observed values. The results closest to the dike (at x=45.96m) also show very promising results. For the low frequency component, a SCI=0.07716 and Rel.bias=0.05495 are very favourable. In contrast, at location x=45.54m, the low frequency results are less good. This can be explained by the changing of the breaker parameter and the friction coefficient. These too have a significant effect on the wave actions close to the dike, especially such low depth in combination with friction. During the sensitivity analysis, it was concluded not possible to have both locations near the dike near-perfect. Therefore, the location closest to the dike was chosen as the primary target for validating the model. Despite this, the SCI and Rel.bias of the location x=45.54m is still well within acceptable boundaries.

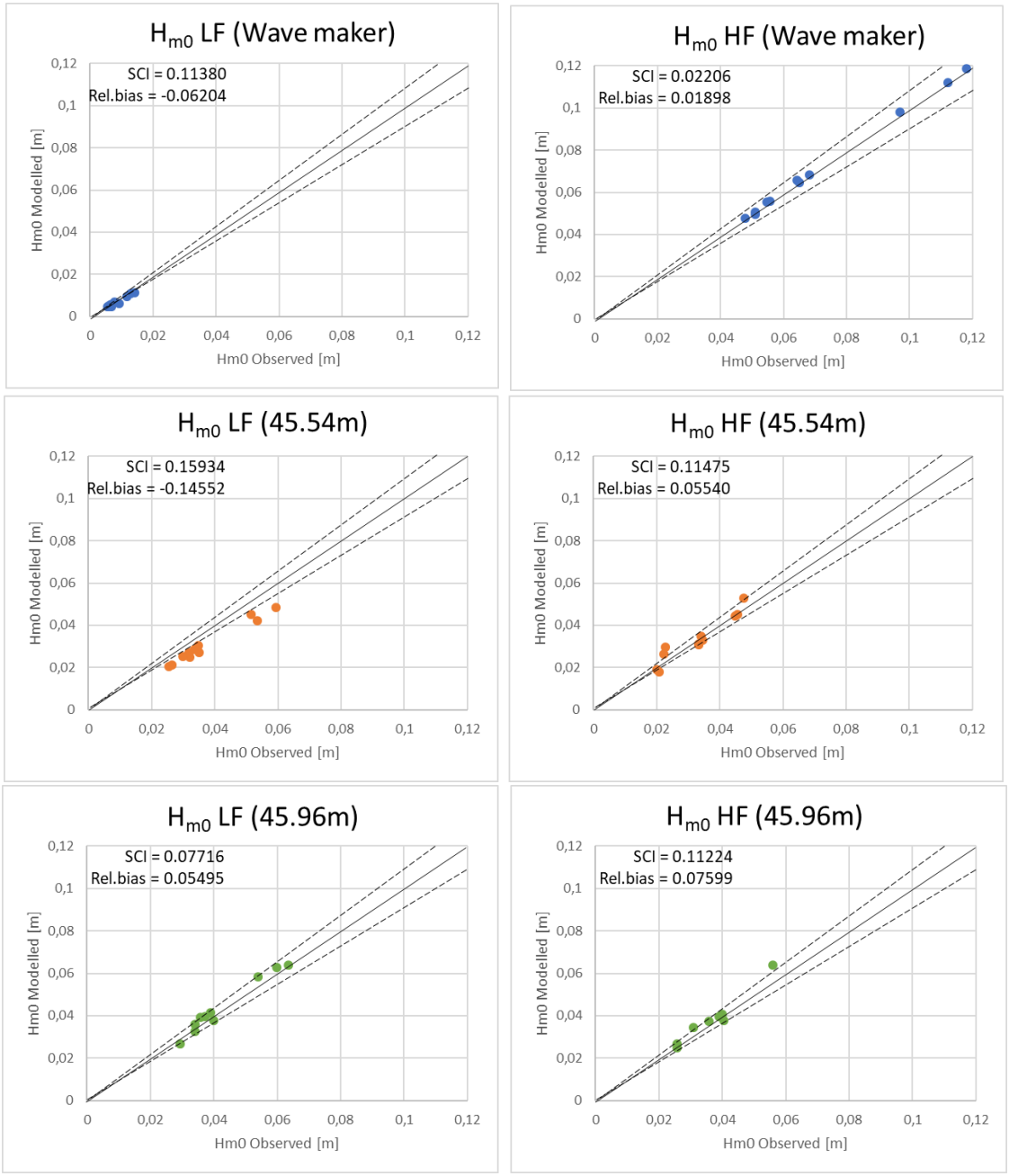

Figure 18. Model validation for $H_{m0,LF}$ and $H_{m0,HF}$

Finally, the IGCs are compared. This is in Figure 19. The same conclusions can be made, the performance is optimal near the wave maker, which means that the initial waves are simulated correctly. Near the dike, the dike, the results are close to reality, but a little off (SCI=0.13096, Rel.bias=-0.12436 and SCI=0.08825, Rel.bias=-0.06072). This could indicate that the wave breaking simulated in SWASH is not exactly as what happened in the lab experiments.

An explanation could be the nature of the dike. As there was no detailed information given, the dike is inputted in the model as part of the bathymetry, rather than a structure. Another hypothesis for this could be the unique lab setup with the partitions between dikes. All things considered, the model still performs well within acceptable boundaries, although underpredicts the low frequency a little.

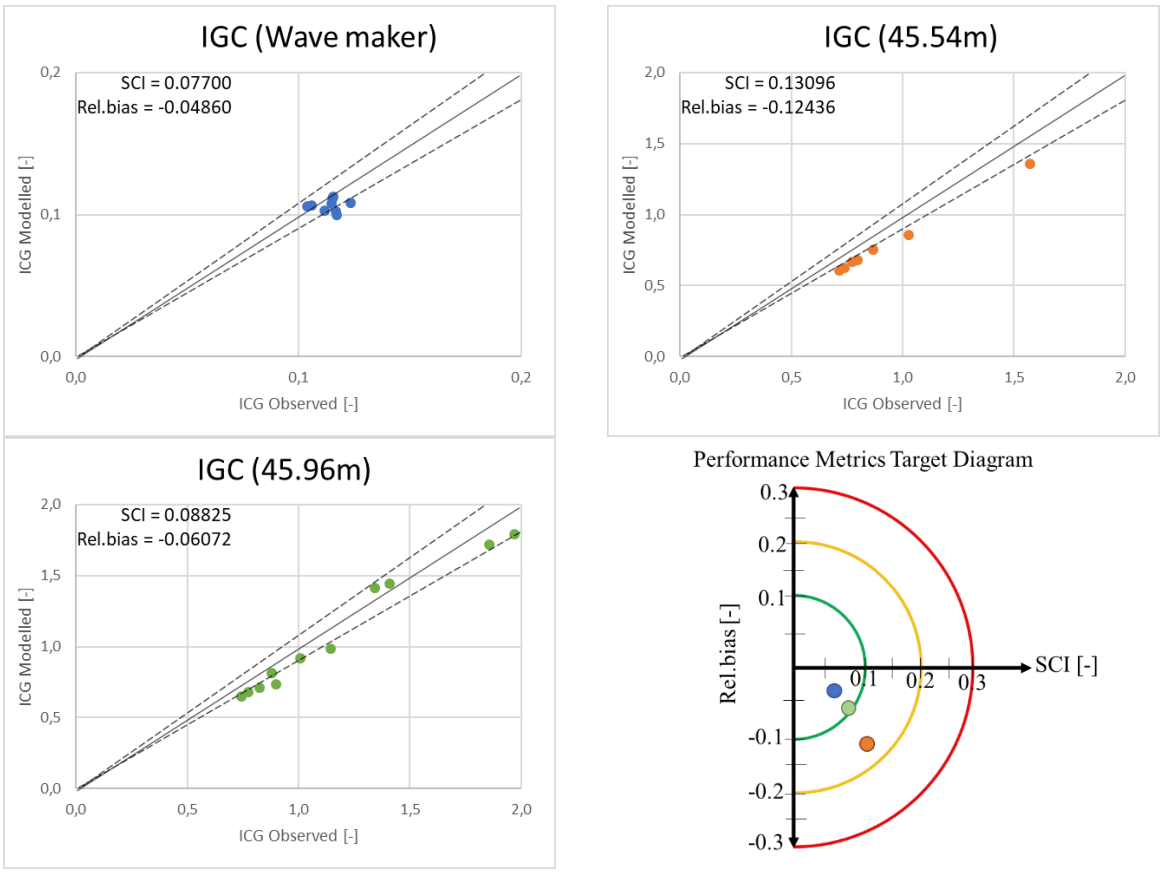

Figure 19. Model validation for IGC.

Furthermore, the water levels have been taken into account. This is done by taking the average value of the water-level time series of each test, both for the lab experiment and the SWASH output. This is then analysed with a RMSE. For all measurements, there is an average RMSE of +0.00156m. This means that SWASH overpredicts the water level, but only by a very small fraction, almost negligible. Therefore, the water level is assumed correct. One example is shown in Figure 20.

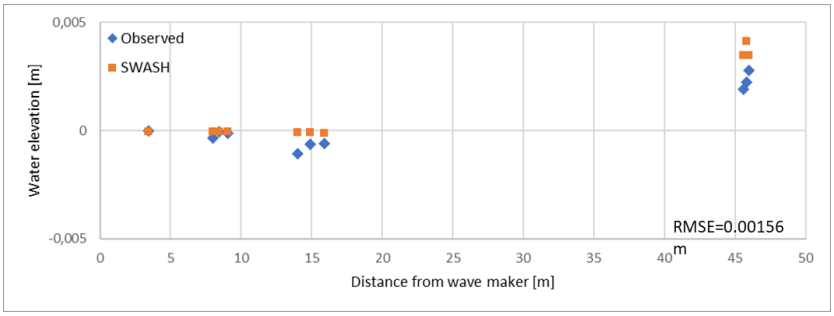

Figure 20. Analysis water level for test 1.

To end the model validation, a visual analysis is done, comparing the wave spectra. In Figure 21, one example is given for test 5. The general conclusion is the same for all tests. The spectra are very similar, comparing the lab observations with SWASH. A main difference, near the wave maker, is that the spectrum of the measured data is more spiked than the SWASH spectrum. One explanation could be that the boundary conditions in SWASH and the lab experiment are not exactly identical. While both have wave absorption, there are no details known about the exact type of wave absorber used in the lab. Therefore, a default boundary condition was used in SWASH. Overall, the spectra are visually similar.

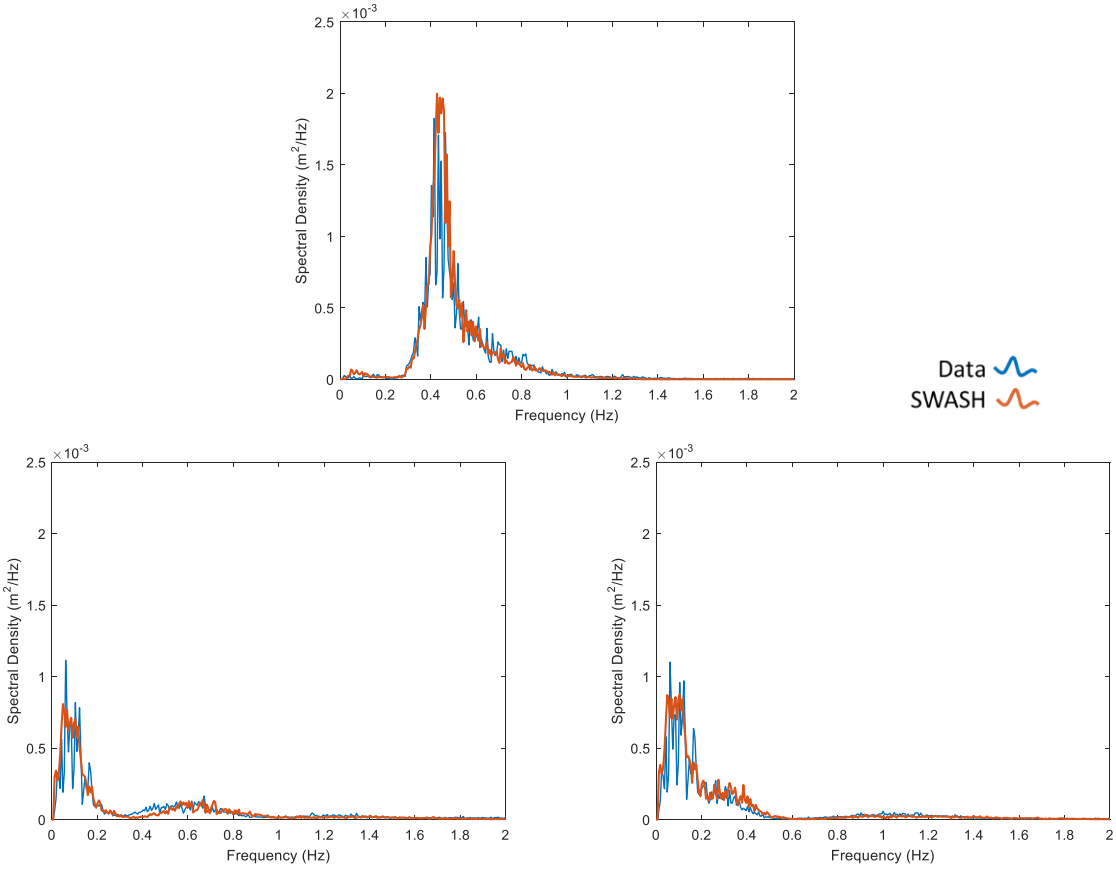

Figure 21. Wave spectra for calibrated SWASH model, test 5.

Everything in this chapter is done to recreate the lab experiment as close as possible in the simulation model, so also using a scaled down version. Starting from the next chapter on, the simulations will happen to approximate real-life conditions. This will not be done anymore on a lab scale, but on a full scale. The scaling up is done using Froude scaling (Heller, 2011) and is shown in Appendix 3.

To finish this chapter, it has to be mentioned that for the lab experiment, there was no vegetation present. Therefore, this parameter cannot be validated and has to be assumed to function correctly, based on previous researched using SWASH in vegetated environments (Torres-Freyermuth *et al.*, 2012; Zijlema, 2012; Cao, Feng and Chen, 2016).

4. Simulations

Now that the model is calibrated, several input parameters can be varied. As mentioned before, four parameters are to be varied in this study:

- Input wave height H_{m0}
- Input wave period T_P
- Bed slope
- Vegetation

These parameters aren't chosen randomly, however. Two field cases have been examined briefly and real-life conditions are chosen to be input in the simulations.

4.1. Field sites

One case is chosen in the north of the Netherlands, namely in the Wadden Sea. The other is chosen on the East Coast of the US, more specific, a part of the Chesapeake Bay. Both will be discussed briefly.

4.1.1. Wadden Sea, Netherlands

The first location is located in the north of the Netherlands. The Wadden Sea is a body of water in between the main land of the Netherlands, Germany and Denmark, and several barrier islands. It could be described as a large system of intertidal sand and mud flats, and is relatively shallow, only having a depth of several meters during high tide. This system is very rich in nature, both fauna and flora. Since there are multiple intertidal areas, the system is rich in seagrasses and saltmarshes (*WaddenZee.nl*, 2016).

Figure 22. Location measurements test site 1.

For the wave conditions in the Wadden Sea, a wave buoy just outside of the barrier islands is chosen. The conditions there can vary from significant wave heights H_{m0} of approximately 1.0 tot 1.5m, while during heavy storm days, wave heights of up to 7m can be achieved (Post *et al.*, 2015).

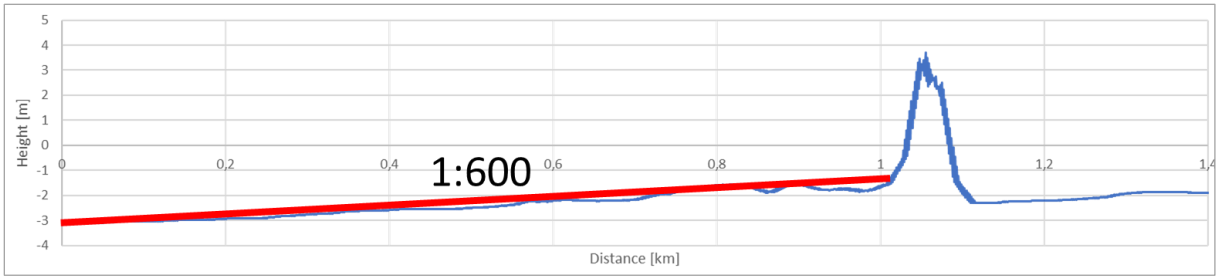

Figure 23. Bathymetry Wadden Sea. A slope of roughly 1:600.

The vegetation can be divided into two categories: sea grass and salt marsh. A list of the species present at the location is given in Table 2:

Table 2. Vegetation parameters Wadden Sea.

Name	Aster Tripolium	Suaeda maritima	Elymus repens	Spartina anglica
Type	Flower (emerged)	Grass (submerged)	Grass (emerged)	Grass (emerged)
Height [m]	0.67	0.42	0.77	0.67
Diameter [m]	0.0089	0.0024	0.0021	0.0056
Vegetation density [stems/m²]	67	231	637	262

Because of the large span in coefficients that represent vegetation drag coefficient, this value is not calculated here, but has been selected based on previous research, and has been chosen to be C_D=0.4 (Vuik *et al.*, 2016).

Figure 24. Vegetation types at the Wadden Sea site. Aster Tripolium (top left), Suaeda maritima (top right), Elymus repens (bottom left), Spartina anglica (bottom right). (Photos by: Vincent Vuik).

4.1.2. Chesapeake Bay, USA

Chesapeake Bay is located on the East Coast of the U.S. as seen on Figure 25. Tectonically, the East coast of the U.S. is considered a trailing edge coast, and Chesapeake Bay is situated somewhere in the middle of the North American Plate. This means that it has a larger continental shelf than the West coast, so swell waves have a longer path to travel and can build up more energy. This however also means that there is a high storm surge potential. This would give waves with a wave height H_{m0} of up to 10m offshore during storms.

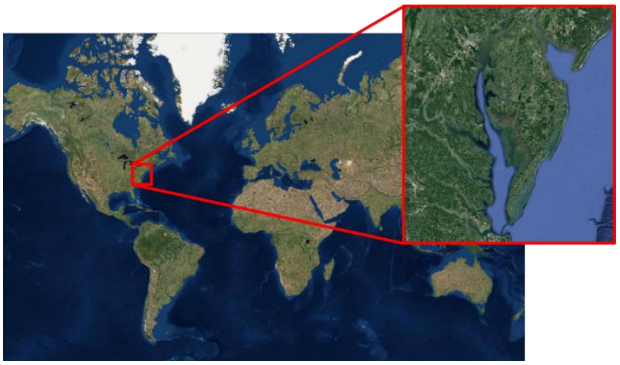

Figure 25. Location of the Chesapeake Bay.

In the large inlet of the bay, a combination of bridges and tunnels was built to make a road network and an easier connection between the northern states around the Chesapeake Bay (Virginia, Delaware and Marylans) and states located south of the bay (also Virginia, and North Carolina).

The Chesapeake Bay is mainly wetlands, were 14% are intertidal salt marshes, and 86% is fresh water wetlands (Chesapeake Bay Program, 2018). There is a very large biodiversity of fauna and flora. The flora consists mainly out of subaquatic saltmarsh seagrasses, saltmarsh plants and fresh water vegetation up in the bay (Dome *et al.*, 2009). The bay itself has been reported for its nature-based flood and erosion control, and has been proven quite effective in natural wave reduction (Narayan *et al.*, 2016).

Table 3. Vegetation parameters Chesapeake Bay.

Name	Spartina alterniflora	Spartina patens
Type	Grass (emerged)	Grass (submerged)
Height [m]	0.7415	0.021
Diameter [m]	0.00538	0.00337
Vegetation density [stems/m²]	344	816

Figure 26. Vegetation types at the Chesapeake Bay. Spartina alterniflora (left) and Spartina patens (right). Photos from (Chesapeake Bay Program, 2018).

4.1.3. Scenarios

Depending on the two different sites, the following parameters have been selected to be varied. For the simulations in SWASH, all possible combinations between these parameters will be made, which results in 625 combinations. Some waves are limited by steepness. A rule of thumb is that the ratio between the wave height and the wave length H_{m0}/L_0 should not exceed 1/7 (Bosboom and Stive, 2015). In this case, the combination of H_{m0}=10.0m and T_P=6.0s is invalid because of the steepness criterion. Also, all scenarios are made without vegetation. The effect of vegetation is only examined on the 1:500 slope.

Table 4. Variation parameters. All possible combinations between the first three columns should be made for all input scenarios. The vegetation is only analysed for the weakest slope.

H_{m0} [m]	T_P [s]	Bed slope [-]
1.0	6.0	1:25
2.0	8.0	1:50
4.0	10.0	1:100
6.0	12.0	1:200
10.0	14.0	1:500

Vegetation
No vegetation
Spartina anglica
Spartina patens
Aster Tripolium

The different slopes are shown in Figure 27.

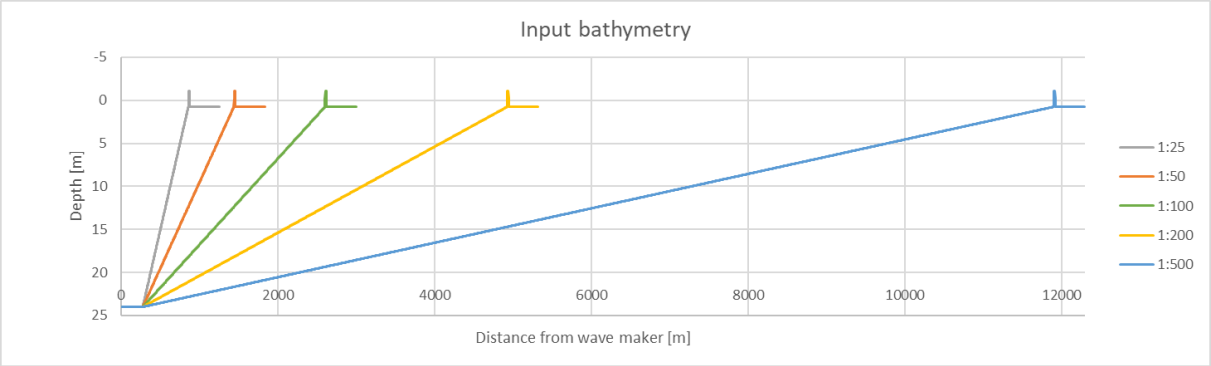

Figure 27. Input topography

The difference between the different vegetation types has been simplified in Figure 28.

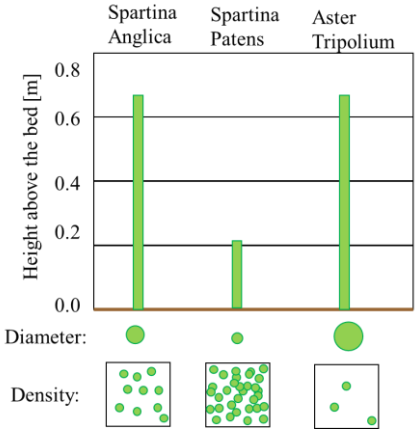

Figure 28. Three selected vegetation types.

The three selected vegetation types are briefly discussed:

- Spartina Anglica, known as common cordgrass, is a long grass with leaves and flowers in spring and summer (however the vegetation data here is measured during winter times). This is common type of plant in the North Sea. From now on, referred to as SPAN.
- Spartina Patens, known as salt meadow cordgrass. This is a very low and very dense seagrass. This is a common species in North America. From now on, referred to as SPPA.
- Aster Tripolium, known as sea aster, is a flower with a wide stem diameter and few plants per square meter. It is commonly found in Europe. Further referred to as ASTR.

In the model runs, the foreshore has been given a width of 400m, which is an average value for a Dutch foreshore (Vuik *et al.*, 2016). This foreshore width is mainly valid for a 1:500 slope, which is closest to the real case. The 1:25 and 1:50 especially are too steep for this kind of vegetation, so will not be used for the vegetation analysis. Furthermore, one constant water level is chosen at a 0.75m, which corresponds to the lab experiments (but scaled up). And a single dike with a slope of 1:2 is chosen, also as seen in the lab experiment.

4.2. Model output

4.2.1. Water level analysis

Before the IG waves are analysed, the water level is examined. This is done by looking into the MWL, or set-up. In here, the results for the 1:500 slope are discussed, because this is closest to the reality at the Wadden Sea and the Chesapeake Bay. Some other results are shown in Appendix 4. Figure 29 shows the cross-shore evolution of the wave height and the water level for two randomly selected tests (H_{m0}=4m, T_P=10s and H_{m0}=10m, T_P=12s). This set-up is calculated by taking the mean value of the water level elevation time series. The still-water level without any wave actions is 0.75m. In other words, the total depth becomes 0.75 added with this set-up.

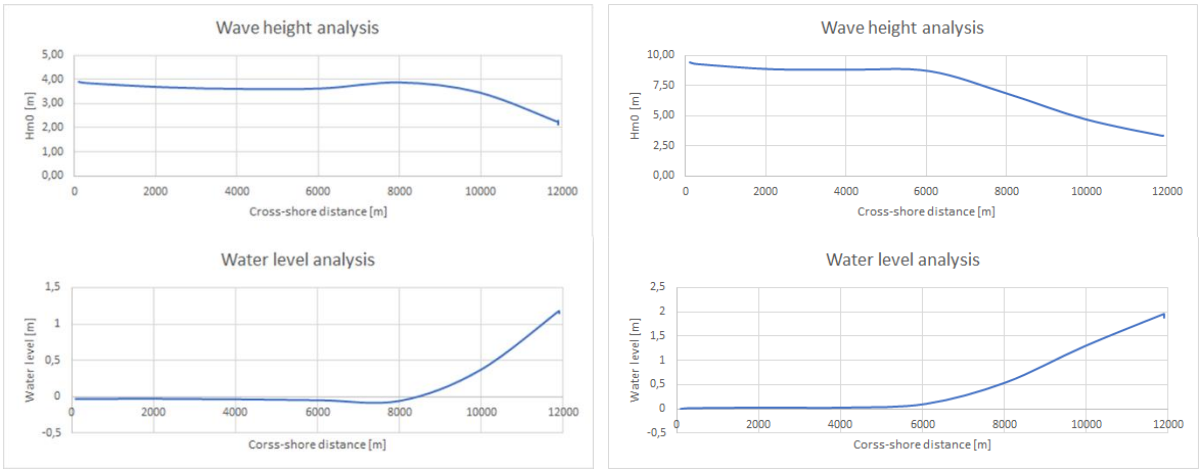

Figure 29. Water level and wave height analysis for H_{m0}=4m, T_P=10s (left) and H_{m0}=10m, T_P=12s (right).

The setup is shown in tables in Appendix 4. To summarise the conclusion, the MWL set-up increases for an increasing incoming wave height. The same conclusion can be made for an increasing wave period and a decrease in slope steepness.

4.2.2. IG analysis

Off course the main focus of this research is the IG component of the waves. This will be analysed periodically per slope first and for the scenarios without vegetation. The plots are all given here, with each plot concerning one of the slopes, and H_{m0} and T_P on the x -and y-axes respectively. The contours represent the IGC. All plots are given at the location of the dike toe.

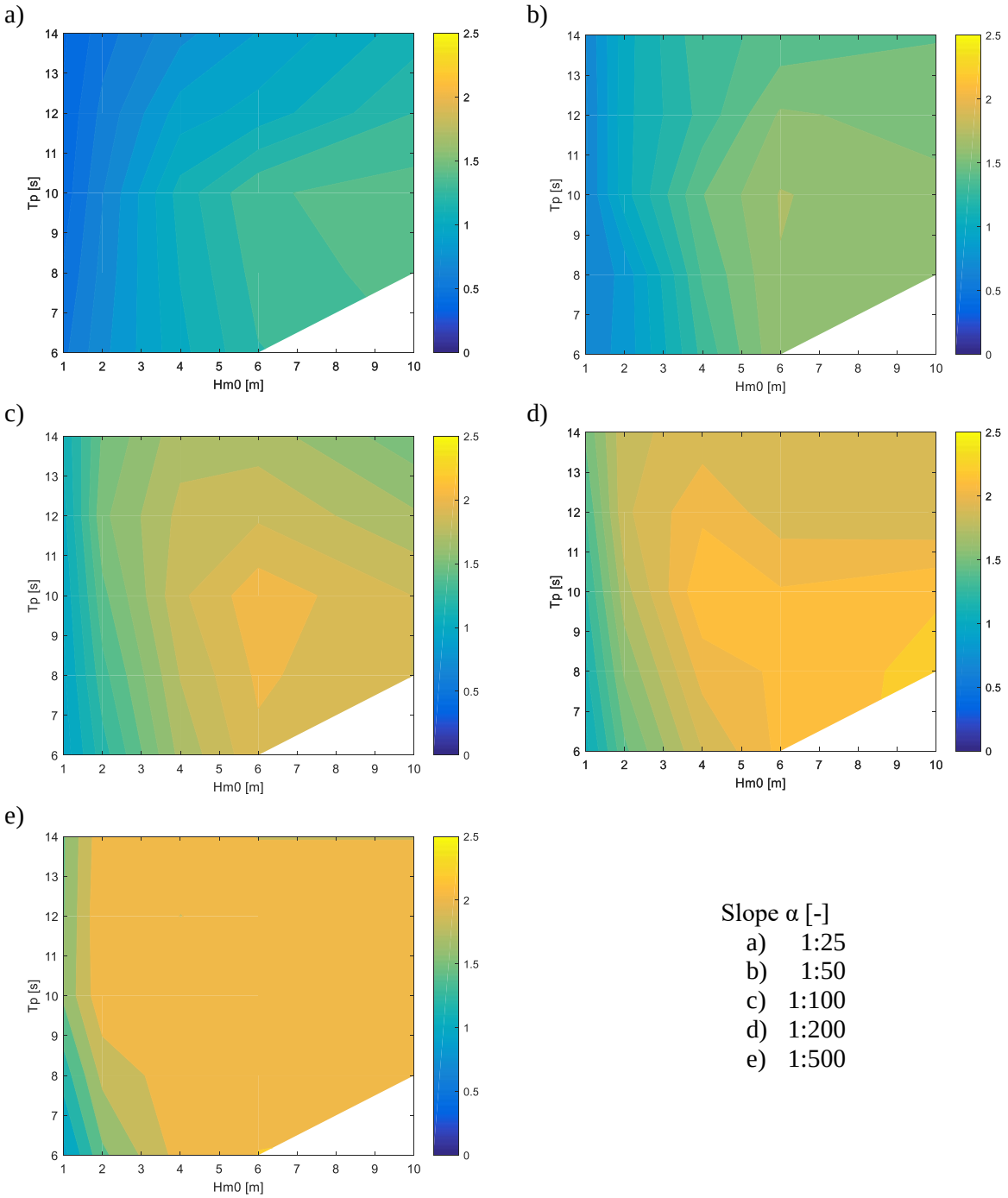

Figure 30. IGC for constant slopes. Plots are taken at the toe of the dike.

The contour plots show the IGC for constant slopes, as a function of the offshore wave height and period. Simply put, a darker blue shows dominance of gravity waves, while a brighter yellow show dominance of IG waves. On first glance, it is clear what a slope does. A steep slope, such as 1:25, has mostly gravity wave dominance. In such case, waves can travel further towards the shore without breaking, so the IG

wave has almost no change to build up. Also for a slope of 1:50, the main dominance is gravity waves. Only for waves with an H_{m0}=4 and larger, IG wave dominace can be noticed. In contrast, for foreshores with a 1:500 slope, almost everywhere has IG dominance, even for the lower wave heights. This is because waves break far offshore, and there is more transition of energy between gravity waves and IG waves. This gives the IG waves the possiblity to develop and propagate towards the shore.

Another evident conclusion is the effect of the offshore wave height. Small waves will result in a smaller IGC. The smaller waves will propagate closer to shore without breaking, therefore the IG wave is either generated later with break point generation, and the bound long wave is released later. This also means that the amplitude growth of the IG wave will be smaller, resulting in a relatively small IG wave.

Analysing the wave periods is a little different. There seems to be a maximum around an offshore peak period of 10 seconds, which mainly occurs together with the higher wave heights, initiating from 6m. However, for the steepest slope (1:500) the IG dominance is practically everywhere.

The dominance of IG waves is determined when the IGC is larger than 1.0, in other words, when the IG part of the total wave height is higher than the gravity part. For values close to 1.0, This could also be seen as a transition zone between gravity and IG dominance. Here, a second scenario is defined, where the IGC is larger than 2.0, which means very IG dominating. Using this, there is no question whether the situation is IG dominating, or more transitioning. The five contour plots given before are summarized in the two plots given in Figure 31, indicating IG dominant and very IG dominant scenarios.

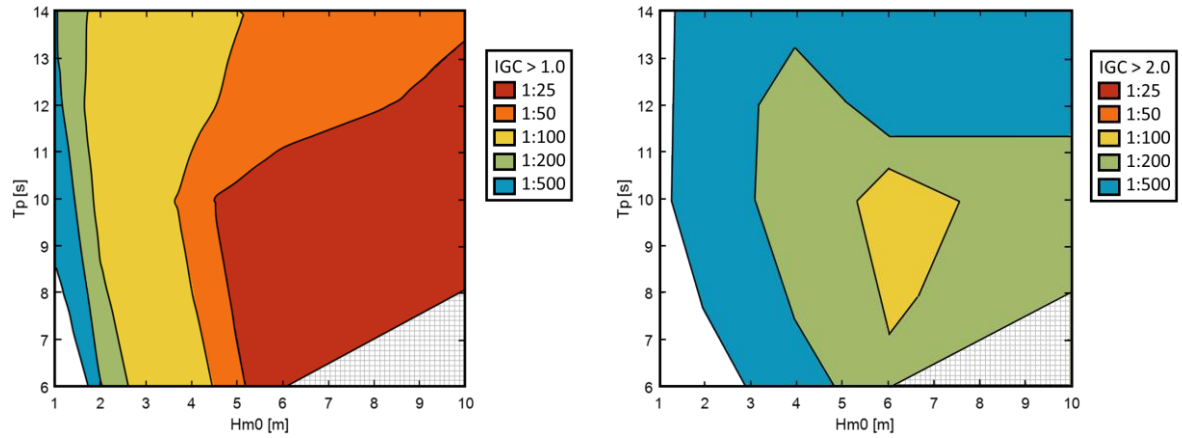

Figure 31. Indication of IG dominance. The left plot indicates IG dominance, the right plot shows very IG dominance. The colours show the different slopes.

In the left plot, where the IGC is larger than 1.0, the same conclusion can be drawn as earlier this chapter: for 1:500 slopes, the IG waves dominate practically everywhere. As the slope gets steeper, the IG dominance disappears for the smaller wave heights. In situations near the steepness limit of waves (bottom right of the contour plots) there is always IG dominance. This situation has the steepest waves, which can result in a very actively breaking sea state. This translates in a lot of IG waves.

Now the right plot, for very IG dominant systems, is analysed. For starters, the steep slopes (1:25 and 1:50) are never very IG dominant. The weakest slope (1:500) is practically everywhere very dominant, except for the lowest wave heights, and the small, short waves. Probably because all this wave energy could be dissipated before it reaches the dike toe. The noticeable part here is that for a 1:100 slope, the very IG dominant system is not near the steepness limit, but about the middle of the figure, with wave heights of 6 to 7m and periods of 7 to 11s. This peak in IG dominance in the middle of the contours is tried to be explained by seiching, for which the calculations can be found in Appendix 5, however this seems unrelated. It has been stated that for weak slopes, waves with low short-wave steepness, the breakpoint forcing of the IG wave is less and the bound long wave shoals together with the short wave

group. Therefor, the freed bound long wave would be larger, but there could be almost no contribution due to the moving breakpoint generation of the waves, which can be seen in the contour plots with weak slopes in Figure 31. For a very steep short-wave regime, the short waves might break at the beginning of the shoaling zone, therefore the bound wave is released very early and may decay while propagating towards the shoreline, however there is more contribution from the moving breakpoint generation of IG waves (Baldock, 2012).

The bed slope parameter (Equation 2.8) indicates the amplitude growth for IG waves. This can be calculated and compared to the output results from SWASH. In Figure 32, the results of this parameter for the steepest and weakest slope are shown:

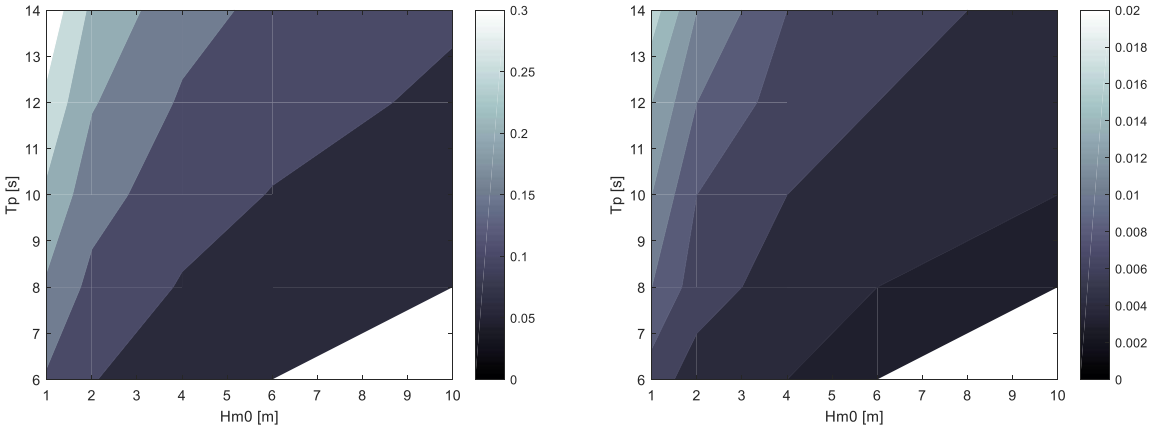

Figure 32. Bed slope parameter for a 1:25 slope (left) and a 1:500 slope (right). Note that the scale bars are not the same.

This explains that for weak slopes, the bed slope parameter will be lower overall than for steep slopes. For weak slopes there is much more possibility for amplitude growth than for steep slopes, where there is insufficient time for the IG wave to grow. The results of the SWASH simulations show confirming results for the lower wave heights but show a more complex pattern for the high wave heights.

4.2.3. Vegetation

The most important slope for all scenarios is 1:500, because that one is closest to the slope of the real-life sites. To limit the amount of data presented here, the main focus for the vegetation will be about the slope of 1:500. Also, a vegetated foreshore for slopes of 1:25 and 1:50 is less likely to exist and these are pretty steep for vegetation to grow.

The main tool for the analysis is the IGC, defined earlier (Equation 3.7). However, this component alone does not tell the whole story. It shows efficiently in what situations the IG part of the waves is larger than the gravity waves, in other words, whether IG waves dominate or not. But it shows no indication of the actual wave height. Especially for vegetated foreshores, the wave height reduction due to vegetation plays an important role, so also for the IG part of the waves. Therefor a second coefficient is chosen, showing the ratio of the IG wave height at the dike toe and the offshore total wave height, here defined as the relative wave height $H_{m0,\,rel.}$, or separated into the low frequency and high frequency wave heights, respectively $H_{m0,\,rel,\,LF}$ or $H_{m0,\,rel,\,HF}$.

$$H_{m0,rel,LF} = \frac{H_{m0,LF,toe}}{H_{m0,total,offshore}} \tag{4.1}$$

And;

$$H_{m0,rel,HF} = \frac{H_{m0,HF,toe}}{H_{m0,total,offshore}} \tag{4.2}$$

Where: $H_{m0,\ LF,\ toe}$ = low-frequency wave height at the dike toe [m]

$H_{m0,\ HF,\ toe}$ = high-frequency wave height at the dike toe [m

$H_{m0,\ total,\ offshore}$ = total offshore wave height [m]

To avoid confusion, the contour plots using the low-frequency wave height at the dike toe will be shown in range from yellow to red, the high-frequency wave height contours will be shown in a range from white to blue, while the IGC will still be shown in a blue to yellow range. The first example is given in Figure 33 for the 1:500 slope.

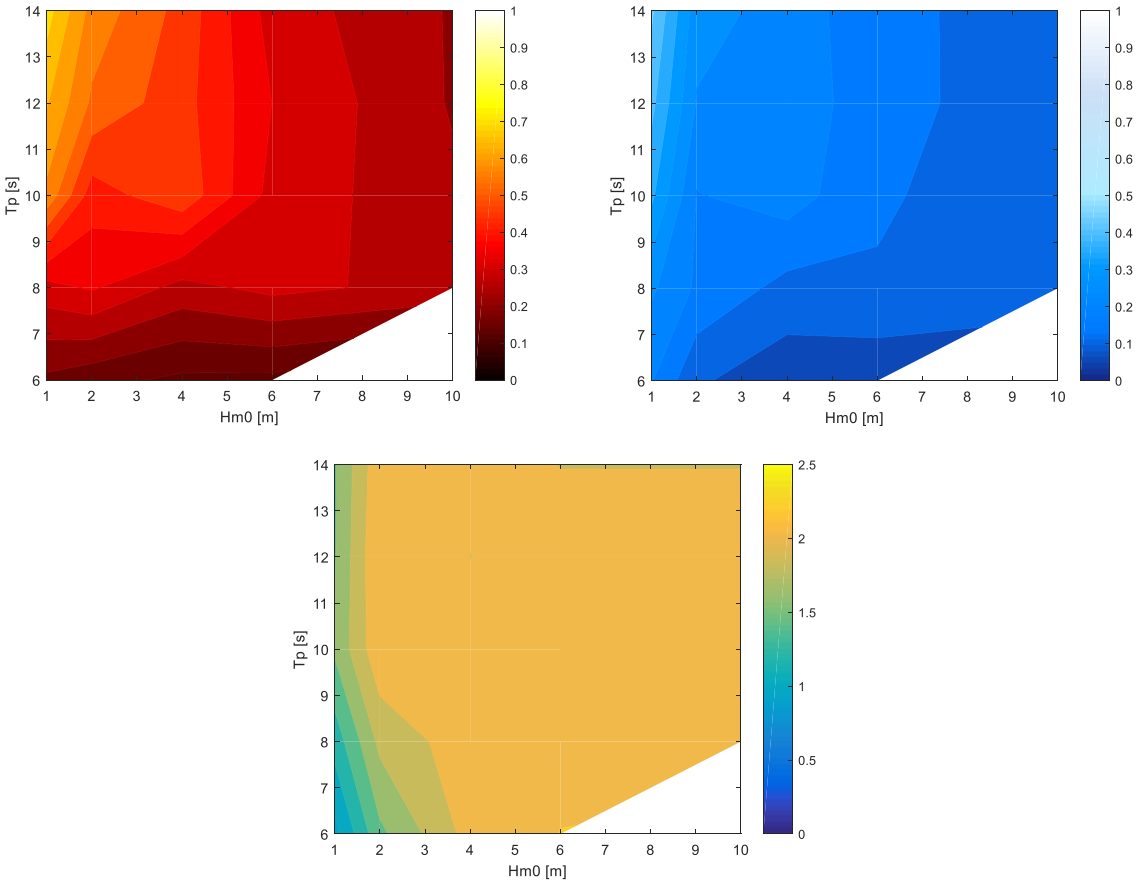

Figure 33. Wave reduction for low frequency (top left), high frequency (top right) and IGC (bottom) for a slope of 1:500 and no vegetation.

Although the bottom plot (IGC) shows that the IG waves dominate practically everywhere, the relative wave heights show that for shorter waves, or lower periods, the IG component of the wave is only a fraction of the total wave height, even no more than 15% for the shortest simulated waves. Probably these waves would break and not even reach the shoreline. The same conclusions can be reached when looking at the high -and low-frequency wave heights, short, low waves dissipate a lot and almost don't reach the shoreline.

Long, low waves (H_{m0}=1m, T_P=14s) show the highest IG and gravity waves, relative to their offshore wave heights. Although 70% of 1m offshore wave height is relatively small, it is important to note that for small waves, the relative size of the IG wave will be large.

The right part of all three figures, so the higher wave heights, show a large IGC, but a smaller (relative) IG wave height. The IG wave height is dissipated more, relative to the offshore wave height, but the IGC is very large, meaning that the gravity waves have been dissipated even more in a weak slope

environment. This shows IG dominance about everywhere, with low-frequency wave heights of about 20% of the offshore wave heights.

Now to introduce vegetation to the scenarios. Three vegetation types are selected, located on the Wadden Sea site and the Chesapeake Bay site. All species are common in salt marshes.

The results of the first vegetation (SPAN) is shown in Figure 34:

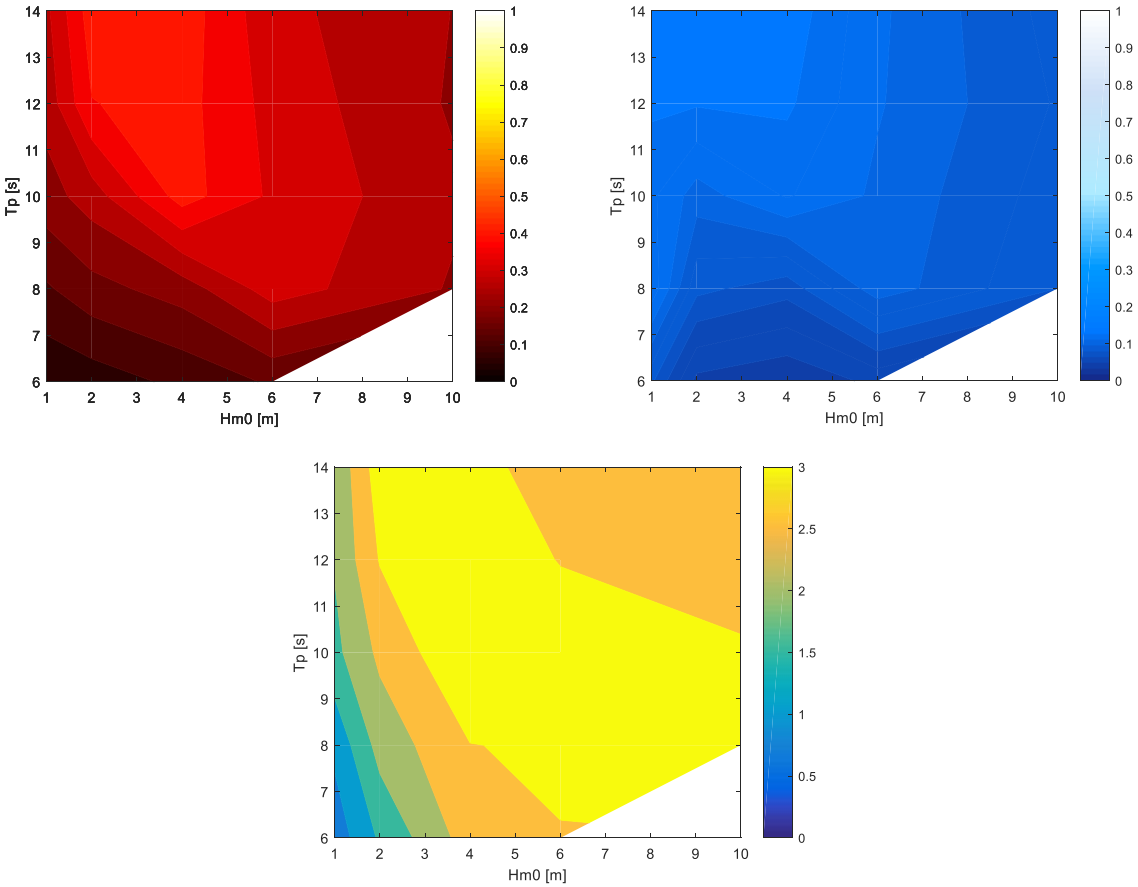

Figure 34. Wave reduction for low frequency (top left), high frequency (top right) and IGC (bottom) for a slope of 1:500 and vegetation type SPAN.

For starters, the reduced wave heights are examined. The low wave heights and the short periods are greatly affected by the vegetation and show a large decrease in IG wave heights. However, in case of the largest and longest waves, they are almost not affected by the vegetation. To compare, some results are summarised in Table 5. For the offshore wave heights, the average relative wave heights at the dike toe are examined. This table illustrates what happens in the transition from no vegetation to vegetation.

For the lowest two offshore wave heights (1 and 2m), the reduction in wave heights from a no vegetation scenario to vegetation, is more or less equal for low -and high frequency wave heights. However, for the higher wave heights, the wave height reduction for high-frequency waves, or gravity waves, becomes much larger than their low-frequency counterparts. Those IG wave heights are barely affected by the vegetation. The largest wave height (10m) is assumed to be so large that the vegetation has a smaller effect, therefore the reduction becomes smaller.

Table 5. Average relative wave heights (LF and HF) with and without vegetation.

$H_{m0,\ offshore}$ [m]	No vegetation		SPAN	
	$H_{m0,\ rel,\ LF}$ [-]	$H_{m0,\ rel,\ HF}$ [-]	$H_{m0,\ rel,\ LF}$ [-]	$H_{m0,\ rel,\ HF}$ [-]
1	0.496	0.372	0.197	0.130
2	0.413	0.226	0.271	0.112
4	0.372	0.205	0.321	0.116
6	0.292	0.158	0.294	0.109
10	0.257	0.122	0.249	0.085

This is also depicted in the IGC, where the high and long waves do show a small increase in IGC, but insignificant compared to other changes. The conclusion here is that the IG dominance is barely affected by vegetation for very large and long waves. For vegetation type SPAN, there seems to be a certain zone on the contour where the IGC is very dominant. This shows that the vegetation is overall good to dissipate gravity waves but has less effect on the IG waves. This severe increase in IGC does not happen for the largest and longest waves, because the vegetation has little effect there. For small waves, the vegetation works well and results in a lower IGC.

Next, the vegetation type SPPA is shown:

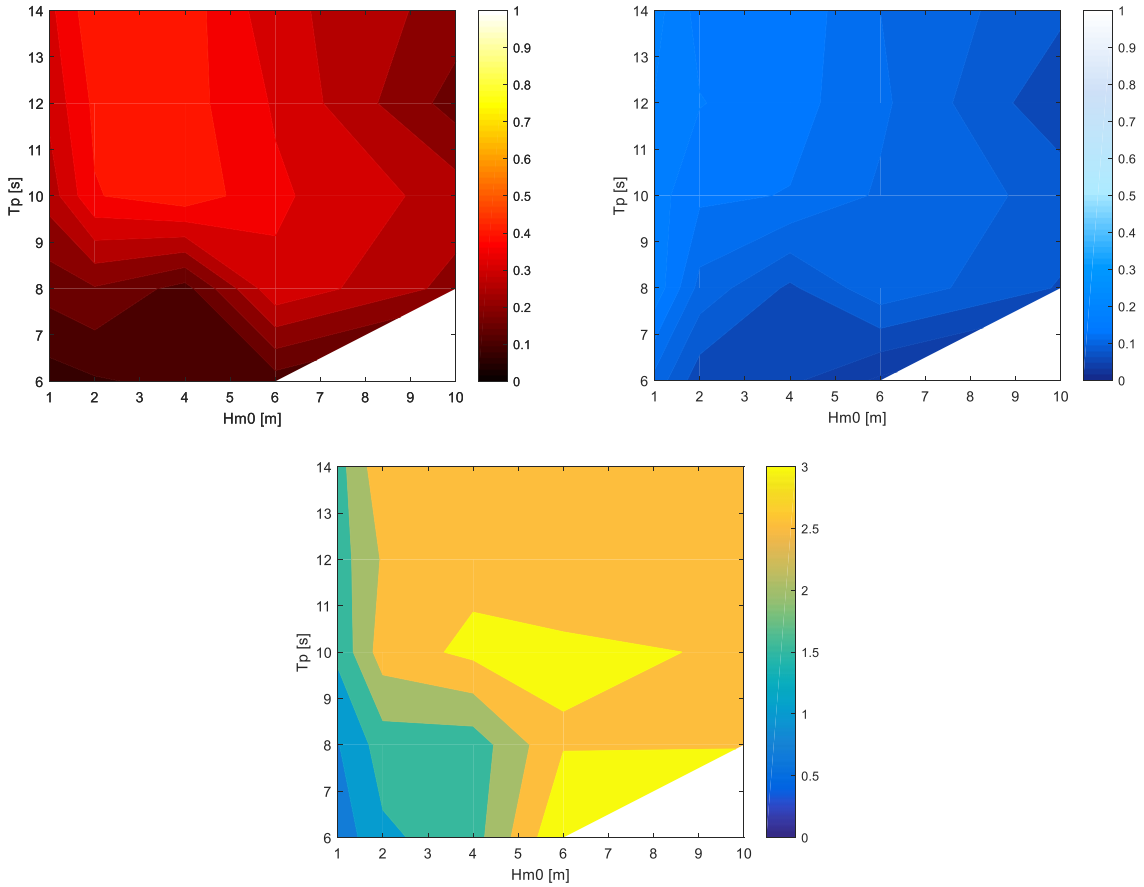

Figure 35. Wave reduction for low frequency (top left), high frequency (top right) and IGC (bottom) for a slope of 1:500 and vegetation type SPPA.

The effect of the low, dense sea grass SPPA is similar to SPAN, but results in a smaller increase of IGC in that zone between very low and very high wave heights. One possible explanation that this vegetation results in a smaller increase in IG dominance, is because the vegetation is lower and finer. As SWASH computes layer per layer, the effect will appear less on the surface, or less in the top layer. However, for

the lowest and shortest wave heights, this vegetation type seems very effective in mitigating the IG dominance.

The third and final vegetation type ASTR is shown next.

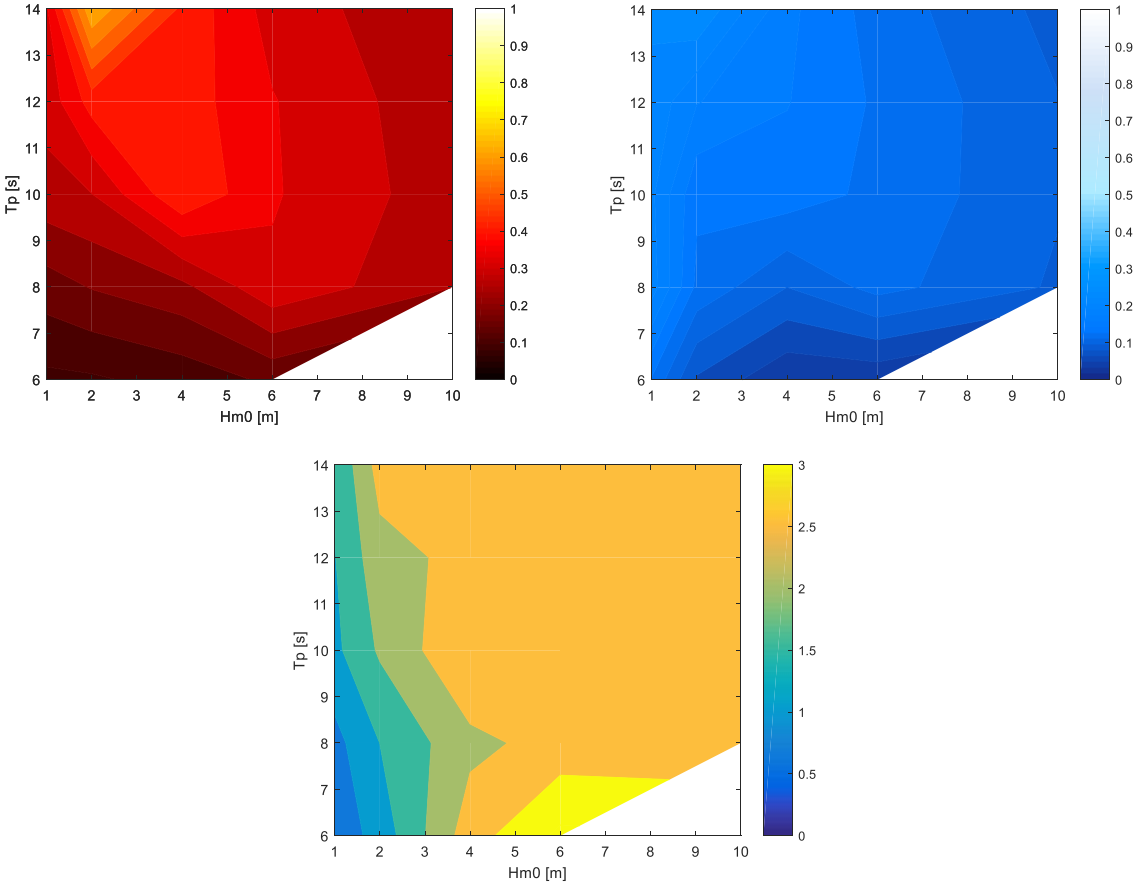

Figure 36. Wave reduction for low frequency (top left), high frequency (top right) and IGC (bottom) for a slope of 1:500 and vegetation type ASTR.

The use of ASTR, a flower with a wide stem diameter seems to be less effective for wave dissipation in general, both in the high -and low frequency bands. However, this flower appears to have a larger effect on the IG waves than the gravity waves for both 1 and 2m input wave heights. It seems to act similar as the other vegetation types for higher wave heights, yet with a smaller effect.

In conclusion, all three plant types seem to be good to dissipate wave energy but are more effective in dissipating gravity waves and less effective on the IG part. For small waves, the vegetation dissipates both the gravity and IG part. For high waves, the gravity part decreases severely, but the IG part seems almost untouched, resulting in more IG dominance.

5. Conclusion

The results of this research will here be summarised and concluded.

5.1. General conclusion

To finish, the research questions are revisited, and it is examined how this study managed to answer them. Starting with some secondary questions:

- What is the optimal run-time versus accuracy equilibrium in SWASH to simulate a large number of scenarios in shallow environment?

A sensitivity analysis was conducted to determine an optimal way of simulating a total of 320 simulations. For SWASH, a grid cell size of 100 cells per wave length was found accurate enough. The difference between 1 and 2 layers gave a significant improvement, but increasing to 3 layers gave a large increase in run-time and barely an increase in accuracy. The default values for the breaking parameter in SWASH was found not accurate in this situation and needed to be increased.

- What is a suitable parameter to analyse the magnitude and/or dominance of infragravity waves over a foreshore.

The focus of this research lies on the dominance of IG waves at the dike toe. The ratio of the low-frequency wave height over the high-frequency wave height, or defined here as the infragravity coefficient (IGC), represents the dominance of IG waves over gravity waves as required. However, this coefficient doesn't show the full story. To give an indication of the wave height, more importantly, the wave height reduction, a second parameter was introduced. This parameter showed either the low -or high-frequency wave height at the dike toe, relative to its offshore wave height.

The main research question:

"Under what combinations of topography, vegetation and offshore conditions do infragravity waves dominate at a dike toe?"

An efficient way of showing multiple scenarios is a contour plot. From these plots, the IG dominance of a coastal system with different combinations can easily be derived. This research question can basically be answered using Figure 37 (excluding the effects of vegetation).

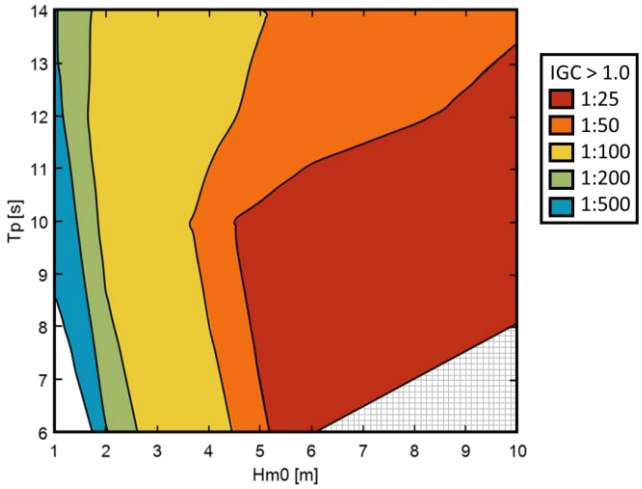

Figure 37. IG dominance at the dike toe.

- The topography is very influential on the IG dominance. The weak slope shows that IG waves dominate almost everywhere. Reducing a slope from 1:500 to 1:200 and even 1:100 only influences the smallest offshore wave heights (1 and 2m). The steepest slopes used for this research (1:50 and 1:25) show IG dominance for higher wave heights and periods, but gravity dominance for smaller wave heights.
- The wave heights show almost a linear trend. Especially for weak slopes, the IG dominance increases almost linearly with increasing wave height. As the slope gets steeper, the combination of high wave heights and long periods leads less and less to IG dominance.
- The wave period shows a maximum value in IG dominance for 10s. Shorter periods are more or less the same, while the IG dominance for longer periods reduces rapidly. This effect occurs for steep slopes mostly and decreases for weaker slopes.

When examining very IG dominant scenarios (IGC>2.0), a steep slope doesn't occur anymore, and the weakest slope (1:500) is still almost everywhere very IG dominant. Coastal systems that are very IG dominant seem to have a center around the combination of H_{m0}=6m and T_P=8 to 10s.

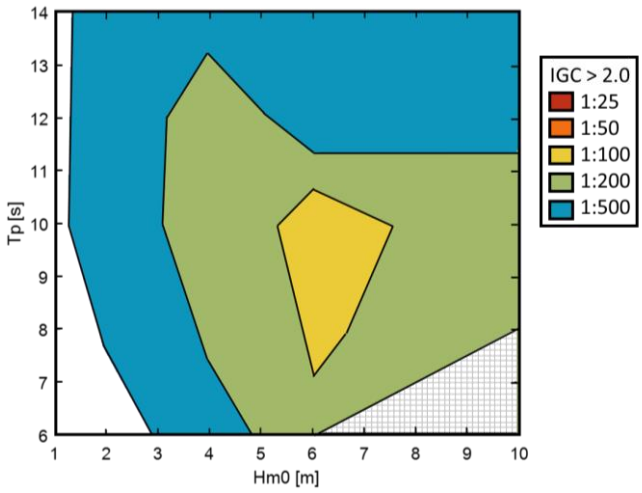

Figure 38. Very IG dominant scenarios at the dike toe.

- What is the effect of different kinds of vegetation on infragravity waves?

Three vegetation types are examined here: cordgrass (Spartina Anglica), salt meadow cordgrass (Spartina Patens) and sea aster (Aster Tripolium), respectively a high sea grass, a submerged and dense sea grass, and a thick-stemmed flower.

The effects of the three types were similar and generally showed a decrease in IG dominance for very low wave heights, almost no change for very high wave heights and a large increase in IG dominance for all in between the lowest and highest wave heights. The vegetation seems to be more efficient in dissipating gravity waves than IG waves. In case of cordgrass, the IG dominance was increased a lot to values of IGC=3.0 for about half of the scenarios. Sea aster seemed to be very effective in reducing the IG dominance for low wave heights.

5.2. Limitations of this research

Throughout this study, the following limitations were identified:

- The sensitivity analysis was conducting comparing to a lab experiment, on a lab scale. The flume for which the experiments were conducted is considered 1D and the outcome of the sensitivity analysis might be considered only valid for 1D-situations.

- The simulation of the multiple scenarios was executed varying only the four selected parameters (slope, H_{m0}, T_P and vegetation). The other parameters, such as the breaker parameter in SWASH and the grid size, were kept the same for all simulations. This might give some inaccuracies in the results.
- The conclusions of this research were made derived from a theoretical study, based only on simulations. The real situations might vary from the scenarios made in this study.

5.3. Recommendation for future research

This research can be extended into future works. Some suggestions are made here:

- This study was made for 1D cases, neglecting longshore effects. The dominance of IG waves in a 2D environment might deviate from this outcome. The performance of SWASH in a 2D simulation might be a good add-on.
- The sensitivity analysis was only conducted on a limited number of parameters (grid size, number of layers, breaker parameter and friction). A wider model calibration could result in output closer to reality.
- Everything done in this research is theoretical and based on idealised scenarios. These contour plots could be confirmed by simulating a field case in SWASH (ideally the two sites this research is based on, namely the Wadden Sea and the Chesapeake Bay).
- This study only focussed on the IG dominance and did not investigate the overtopping or run-up on a dike. Using a similar strategy of simulating different scenarios could be interesting to determine the effect of IG waves, or IG dominance, on overtopping and run-up.

References

Airy, G. B. (1845) 'Tides and waves', *Encyclopaedia Metropolitana*. London, pp. 241–396.

Altomare, C., Suzuki, T., Chen, X., Verwaest, T. and Kortenhaus, A. (2016) 'Wave overtopping of sea dikes with very shallow foreshores', *Coastal Engineering*. Elsevier B.V., 116, pp. 236–257.

Anderson, M. E. and Smith, J. M. (2013) 'Wave attenuation by flexible, idealized saltmarsh vegetation', *Coastal Engineering*, 53(9), pp. 1689–1699.

de Bakker, A. T. M., Tissier, M. F. S. and Ruessink, B. G. (2015) 'Beach steepness effects on nonlinear infragravity-wave interactions: A numerical study', *Journal of Geophysical Research: Oceans*, 121, pp. 554–570.

Baldock, T. E. (2012) 'Dissipation of incident forced long waves in the surf zone — Implications for the concept of " bound " wave release at short wave breaking', *Coastal Engineering*. Elsevier B.V., 60, pp. 276–285.

Battjes, J. A., Bakkenes, H. J., Janssen, T. T. and Van Dongeren, A. R. (2004) 'Shoaling of subharmonic gravity waves', *Journal of Geophysical Research*, 109, pp. 1–15.

Bertin, X., de Bakker, A., Van Dongeren, A., Coco, G., André, G., Ardhuin, F., Bonneton, P., Bouchette, F., Castelle, B., Crawford, W. C., Davidson, M., Deen, M., Dodet, G., Guérin, T., Inch, K., Leckler, F., Mccall, R., Muller, H., Olabarrieta, M., Roelvink, D., Ruessink, G., Sous, D., Stutzmann, É. and Tissier, M. (2018) 'Infragravity waves : From driving mechanisms to impacts', *Earth-Science Reviews*. Elsevier, 177, pp. 774–799.

Bertin, X. and Olabarrieta, M. (2016) 'Relevance of infragravity waves in a wave-dominated inlet', *Journal of Geophysical Research: Oceans*, 121, pp. 5418–5435.

Bosboom, J. and Stive, M. J. F. (2015) *Coastal Dynamics I (lecture notes CIE4305)*. 0.5. Delft Academic Press.

Brooks, N., Nicholls, R. J. and Haii, J. (2006) 'Sea Level Rise: Coastal Impacts and Responses', *Norwich WBGU*.

Cao, H., Feng, W. and Chen, Y. (2016) 'Numerical Modeling of Wave Transformation and Runup Reduction by Coastal Vegetation of the South China Sea', *Journal of Coastal Research*, 75(1), pp. 830–835.

Chesapeake Bay Program (2018) *Wetlands*. Available at: https://www.chesapeakebay.net/issues/wetlands (Accessed: 2 March 2018).

CIRIA (2013) *The International Levee Handbook*. London: CIRIA.

CUR, CIRIA and CETMEF (2007) *The Rock Manual. The use of rock in hydraulic engineering.* 2nd edn, *The Rock Manual*. 2nd edn. London: CIRIA.

Dalrymple, R. A., Asce, M., Kirby, J. T., Hwang, P. A. and ASCE (1984) 'Energy balance of wind waves as a function of the bottom friction formulation', *Journal of waterway, port, coastal and ocean engineering*, 110(1), pp. 67–79.

Dean, R. G. and Bender, C. J. (2006) 'Static wave setup with emphasis on damping effects by vegetation and bottom friction', *Coastal Engineering*, 53, pp. 149–156.

Dome, S., Lewis, M., Moran, R. and Nyman, D. (2009) *Chesapeake Bay Wetlands*. Available at: http://academic.emporia.edu/aberjame/student/moran6/report1.htm.

Van Dongeren, A., Battjes, J., Janssen, T., Noorloos, J. Van, Steenhauer, K., Steenbergen, G. and Reniers, A. (2007) 'Shoaling and shoreline dissipation of low-frequency waves', *Journal of Geophysical*

Research, 112, pp. 1–15. doi: 10.1029/2006JC003701.

Van Dongeren, A., Lowe, R., Pomeroy, A., Trang, D. M., Roelvink, D., Symonds, G. and Ranasinghe, R. (2013) 'Numerical modeling of low-frequency wave dynamics over a fringing coral reef', *Coastal Engineering*. Elsevier B.V., 73, pp. 178–190.

Van Dongeren, A., Reniers, A. and Battjes, J. (2003) 'Numerical modeling of infragravity wave response during DELILAH', *Journal of Geophysical Research*, 108, pp. 1–19.

Fiedler, J. W., Smit, P. B., Brodie, K. L., McNinch, J. and Guza, R. T. (2018) 'Numerical modeling of wave runup on steep and mildly sloping natural beaches', *Coastal Engineering*. Elsevier Ltd, 131(November 2017), pp. 106–113.

van Gent, M. R. A. (1999) 'Physical model investigations on coastal structures with shallow foreshores. 2D model tests with single and double-peaked wave energy spectra.', p. 35.

Gomes da Silva, P., Medina, R., González, M. and Garnier, R. (2018) 'Infragravity swash parameterization on beaches : The role of the pro fi le shape and the morphodynamic beach state', *Coastal Engineering*, 136(August 2017), pp. 41–55.

Guza, R. T. and Davis, R. E. (1974) 'Excitation of edge waves by waves incident on a beach', *Journal of Geophysical Research*, 79(9), pp. 1285–1291.

Hatzikyriakou, A., Lin, N., Gong, J., Xian, S., Hu, X. and Kennedy, A. (2016) 'Component-Based Vulnerability Analysis for Residential Structures Subjected to Storm Surge Impact from Hurricane Sandy', *Natural Hazards Review*, 17(1), pp. 1–15.

Hedberg, N., Stenson, I., Kautsky, N., Hellström, M. and Tedengren, M. (2017) 'Causes and consequences of spatial links between sea cage aquaculture and coral reefs in Vietnam', *Aquaculture*, 481(December 2016), pp. 245–254.

Heller, V. (2011) 'Scale effects in physical hydraulic engineering models', *Journal of Hydraulic Research*, 49(3), pp. 293–306.

Hewageegana, V. H., Reniers, A. J. H. M., Van Dongeren, A. R., Tissier, M. F. S., den Heijer, C., Dijkstra, J. T., Nederhoff, C. M. K. and Pearson, S. G. (2017) *Wave Transformation Through Mangrove Coasts - A Model Study with XBeach-Surfbeat*. TU Delft.

Holthuijsen, L. H. (2007) *Waves in Oceanic and Coastal Waters*. New York: Cambridge University Press.

Hu, Z., Suzuki, T., Zitman, T., Uittewaal, W. and Stive, M. (2014) 'Laboratory study on wave dissipation by vegetation in combined current – wave fl ow', *Coastal Engineering*. Elsevier B.V., 88, pp. 131–142.

Inch, K., Davidson, M., Masselink, G. and Russell, P. (2017) 'Observations of nearshore infragravity wave dynamics under high energy swell and wind-wave conditions', *Continental Shelf Research*. Elsevier Ltd, 138(August 2016), pp. 19–31.

Jadhav, R. and Chen, Q. (2012) 'Field Investigation of Wave Dissipation Over Salt Marsh Vegetation During Tropical Cyclone', *Coastal Engineering Proceedings*, pp. 1–11.

Keefer, M. N., Jonkman, S., Vuik, V. and Bricker, J. (2017) *Wetlands as a nature-based flood defense: Numerical modeling of wave attenuation by vegetation in coastal New Jersey*. TU Delft.

LaCasce, J. H. (2008) *A Brief Introduction to Atmospheric Dynamics*.

Lashley, C. H., Roelvink, D., Van Dongeren, A., Buckley, M. L. and Lowe, R. J. (2018) 'Nonhydrostatic and surfbeat model predictions of extreme wave run-up in fringing reef environments', *Coastal Engineering*. Elsevier Ltd, 137, pp. 11–27.

List, J. H. (1992) ‘A model for the generation of two-dimensional surf beat’, *Journal of Geophysical Research*, 97, pp. 5623–5635.

Longuet-Higgins, M. S. and Stewart, R. W. (1962) ‘Radiation stress and mass transport in gravity waves , with application to “ surf beats ”’, *Journal of Fluid Mechanics*, 13, pp. 52–562.

Longuet-Higgins, M. S. and Stewart, R. W. (1964) ‘Radiation stresses in water waves; a physical discussion, with applications’, *Deep Sea Research*, 11, pp. 529–562.

Ma, G., Su, S., Liu, S. and Chu, J. (2014) ‘Numerical simulation of infragravity waves in fringing reefs using a shock-capturing non-hydrostatic model’, *Ocean Engineering*. Elsevier, 85, pp. 54–64.

Masselink, G. (1995) ‘Group bound long waves as a source of infragravity energy in the surf zone’, *Continental Shelf Research*, 15(13), pp. 1525–1547.

Mazarakis, N., Kotroni, V., Lagouvardos, K. and Bertotti, L. (2012) ‘High-resolution wave model validation over the Greek maritime areas’, *Natural Hazards and Earth System Sciences*, 12(11), pp. 3433–3440.

Van der Meer, J. W., Allsop, N. W. H., Bruce, T., De Rouck, J., Kortenhaus, A., Pullen, T., Schüttr umpf, H., Troch, P. and Zanuttigh, B. (2016) ‘EurOtop Manual on wave overtopping of sea defences and related structures. An overtopping manual largely based on European research, but for worldwide application.’, p. 252.

Le Méhauté, B. (1969) *An Introduction to Hydrodynamics and Water Waves*. Miami: Environmental Science Services Administration.

Mendez, F. J. and Losada, I. J. (2004) ‘An empirical model to estimate the propagation of random breaking and nonbreaking waves over vegetation fields’, *Coastal Engineering*, 51, pp. 103–118.

Méndez, F. J., Losada, I. J. and Losada, M. A. (1999) ‘Hydrodynamics induced by wind waves in a vegetation field’, *Journal of Geophysical Research*, 104(August 15), pp. 18383–18396.

Mentaschi, L., Besio, G., Cassola, F. and Mazzino, A. (2013) ‘Problems in RMSE-based wave model validations’, *Ocean Modelling*, 72, pp. 53–58.

Millennium Ecosystem Assessment (2005) *Ecosystems and Human Well-Being*. Washington, DC: Island Press.

Munk, W. H. (1949) ‘Surf Beats’, *Eos Transaction*, 30(6), pp. 849–854.

Narayan, S., Beck, M. W., Reguero, B. G., Losada, I. J., van Wesenbeeck, B., Pontee, N., Sanchirico, J. N., Ingram, J. C., Lange, G.-M. and Burks-copes, K. A. (2016) ‘The Effectiveness , Costs and Coastal Protection Benefits of Natural and Nature- Based Defences’, *PLoS ONE*, 11(5).

Narayan, S., Beck, M. W., Wilson, P., Thomas, C. J., Shepard, C. C., Reguero, B. G., Franco, G., Ingram, J. C. and Trespalacios, D. (2017) ‘The Value of Coastal Wetlands for Flood Damage Reduction in the Northeastern USA’, *Scientific Reports*. Springer US, (August), pp. 1–12.

van der Nat, A., Vellinga, P., Leemans, R. and Slobbe, E. Van (2016) ‘Ranking coastal flood protection designs from engineered to’, *Ecological Engineering*. Elsevier B.V., 87, pp. 80–90.

Nicholls, R. J. (2004) ‘Coastal flooding and wetland loss in the 21st century : changes under the SRES climate and socio-economic scenarios’, *Global Environmental Change*, 14, pp. 69–86.

Nicholls, R. J., Hoozemans, F. M. J. and Marchand, M. (1999) ‘Increasing flood risk and wetland losses due to global sea-level rise: regional and global analyses’, *Global Environmental Change*, 9, pp. 69–87.

Paul, M. and Amos, C. L. (2011) ‘Spatial and seasonal variation in wave attenuation over Zostera noltii’, *Journal of Geophysical Research: Oceans*, 116(8), pp. 1–16.

Peruzzo, P., de Serio, F., Defina, A. and Mossa, M. (2018) ‘Wave height attenuation and flow resistance

due to emergent or near-emergent vegetation', *Water (Switzerland)*, 10(4).

Post, T. M. I., Vuik, V., Borsje, B. W. and Hulscher, S. J. H. M. (2015) *Assessment of wave run-up reductions by salt marshes*. University of Twente.

Reniers, A. J. H. M., Van Dongeren, A. R., Battjes, J. A. and Thornton, E. B. (2002) 'Linear modeling of infragravity waves during Delilah', *Journal of Geophysical Research*, 107(March). doi: 10.1029/2001JC001083.

Roeber, V. and Bricker, J. D. (2015) 'Destructive tsunami-like wave generated by surf beat over a coral reef during Typhoon Haiyan', *Nature Communications*. Nature Publishing Group, 6, pp. 1–9.

Roelvink, D., Mccall, R., Mehvar, S., Nederhoff, K. and Dastgheib, A. (2017) 'Improving predictions of swash dynamics in XBeach : The role of groupiness and incident-band runup', *Coastal Engineering*. The Authors, (February), pp. 1–21.

Roelvink, D., Reniers, A., Van Dongeren, A., van Thiel de Vries, J., Mccall, R. and Lescinski, J. (2009) 'Modelling storm impacts on beaches , dunes and barrier islands', *Coastal Engineering*. Elsevier B.V., 56(11–12), pp. 1133–1152.

Scandurra, G., Romano, A. A., Ronghi, M. and Carfora, A. (2018) 'On the vulnerability of Small Island Developing States : A dynamic analysis', *Ecological Indicators*. Elsevier, 84(June 2017), pp. 382–392.

Scott-Pomerantz, C. D. (2004) *The K-Epsilon Model in the Theory of Turbulence*.

Smith, J. M., Bryant, M. A. and Wamsley, T. V (2016) 'Wetland buffers: numerical modeling of wave dissipation by vegetation', *Earth Surface Processes and Landforms*, 41, pp. 847–854.

Sorensen, R. (2013) *Basic Coastal Engineering*. 2nd edn. Springer Science & Business Media.

Stockdon, H. F., Holman, R. A., Howd, P. A. and Sallenger, A. H. (2006) 'Empirical parameterization of setup , swash , and runup', *Coastal Engineering*, 53, pp. 573–588.

STW (2016) *All-Risk: Implementation of new risk standards in the Dutch flood protection program*, *Perspectief*.

Su, S. and Ma, G. (2018) 'Modeling two-dimensional infragravity motions on a fringing reef', *Ocean Engineering*. Elsevier Ltd, 153(December 2017), pp. 256–267.

Su, S., Ma, G. and Hsu, T. (2015) 'Boussinesq modeling of spatial variability of infragravity waves on fringing reefs', *Ocean Engineering*. Elsevier, 101, pp. 78–92. doi: 022.

Symonds, G., Huntley, D. A. and Bowen, A. J. (1982) 'Two-dimensional surf beat: Long wave generation by a time-varying breakpoint', *Journal of Geophysical Research*, 87(1), pp. 492–498.

The SWASH team (2017) *SWASH user manual*. Delft: Delft University of Technology.

Torres-Freyermuth, A., Mariño-Tapia, I., Coronado, C., Salles, P., Medellín, G., Pedrozo-Acuña, A., Silva, R., Candela, J. and Iglesias-Prieto, R. (2012) 'Wave-induced extreme water levels in the Puerto Morelos fringing reef lagoon', *Natural Hazards and Earth System Science*, 12(12), pp. 3765–3773.

Tuholske, C., Tane, Z., López-Carr, D., Roberts, D. and Cassels, S. (2017) 'Thirty years of land use/cover change in the Caribbean: Assessing the relationship between urbanization and mangrove loss in Roatán, Honduras', *Applied Geography*, 88, pp. 84–93.

UNEP (2014) *GRID-Arendal*. Available at: http://old.grida.no (Accessed: 1 March 2018).

UNEP-WCMC (2017) *Ocean Data Viewer*. Available at: http://data.unep-wcmc.org (Accessed: 1 March 2018).

United Nations (2004) *Guidelines for Reducing Flood Losses*. Available at: https://sustainabledevelopment.un.org/content/documents/flood_guidelines.pdf.

United Nations (2016) *The World's Cities in 2016*.

US Army Corps of Engineers (2015) *Use of Natural and Nature-Based Features (NNBF) for Coastal Resilience*.

Vuik, V., Jonkman, S., Borsje, B. W. and Suzuki, T. (2016) 'Nature-based flood protection: The efficiency of vegetated foreshores for reducing wave loads on coastal dikes', *Coastal Engineering*. Elsevier B.V., 116, pp. 42–56.

WaddenZee.nl (2016). Available at: https://www.waddenzee.nl (Accessed: 6 May 2018).

Whitham, G. B. (1974) *Linear and nonlinear waves*. New York, Wiley.

Xian, S., Yin, J., Lin, N. and Oppenheimer, M. (2018) 'Influence of risk factors and past events on flood resilience in coastal megacities: Comparative analysis of NYC and Shanghai', *Science of the Total Environment*. Elsevier B.V., 610–611, pp. 1251–1261.

Zijlema, M. (2012) 'Modelling wave transformation across a fringing reef using SWASH', *33th International Conference on Coastal Engineering*, 26.

Zijlema, M., Stelling, G. and Smit, P. (2011) 'SWASH : An operational public domain code for simulating wave fi elds and rapidly varied fl ows in coastal waters', *Coastal Engineering*. Elsevier B.V., 58(10), pp. 992–1012.

Appendices

Appendix 1: Rough sensitivity analysis.

Grid size analysis

For starters. the input grid is examined. This indicates the accuracy of SWASH in this situation. Several scenarios are considered. The SWASH manual suggests 50 to 100 grid cells per wave length (The SWASH team, 2017), while from professional experience. a cell size of 2.5cm is suggested.

To analyse the one correct result. the wave height H_{m0} generated by the wave maker is compared to the one from the measured data with a simple error calculation and averaged over all results. This is done for all tests. The averaged result is seen in Table 6:

Table 6. Sensitivity analysis grid size.

Grid cell size [cm]	Number of cells	Runtime [min]	Position 1 (x=3.415m) Error H_{m0} [%]	Position 2 (x=15.54m) Error H_{m0} [%]
1.0	6400	22	1.45	1.12
2.5	2600	8	0.28	-1.47
7.5	1000	2.5	-0.74	-2.92
15	500	1.5	1.42	3.16
50	128	>1	11.79	-14.42

Also the runtime is taken into account. For the increase of grid cells. a linear trend can be seen. Note that this analysis was made on a personal computer, so the result can be different from high-performance simulating systems.

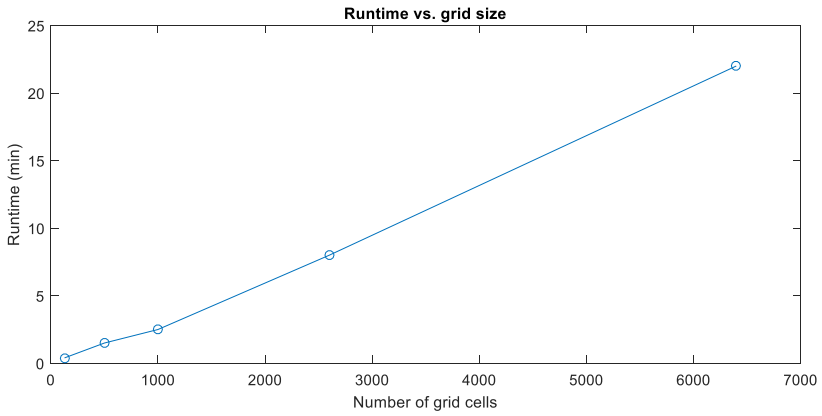

Figure 39. Analysis of the increased runtime for an increased number of cells.

The results here are also compared with the measured data visually using the wave spectra. Here, the plots of test 5 are presented for all five grid sizes.

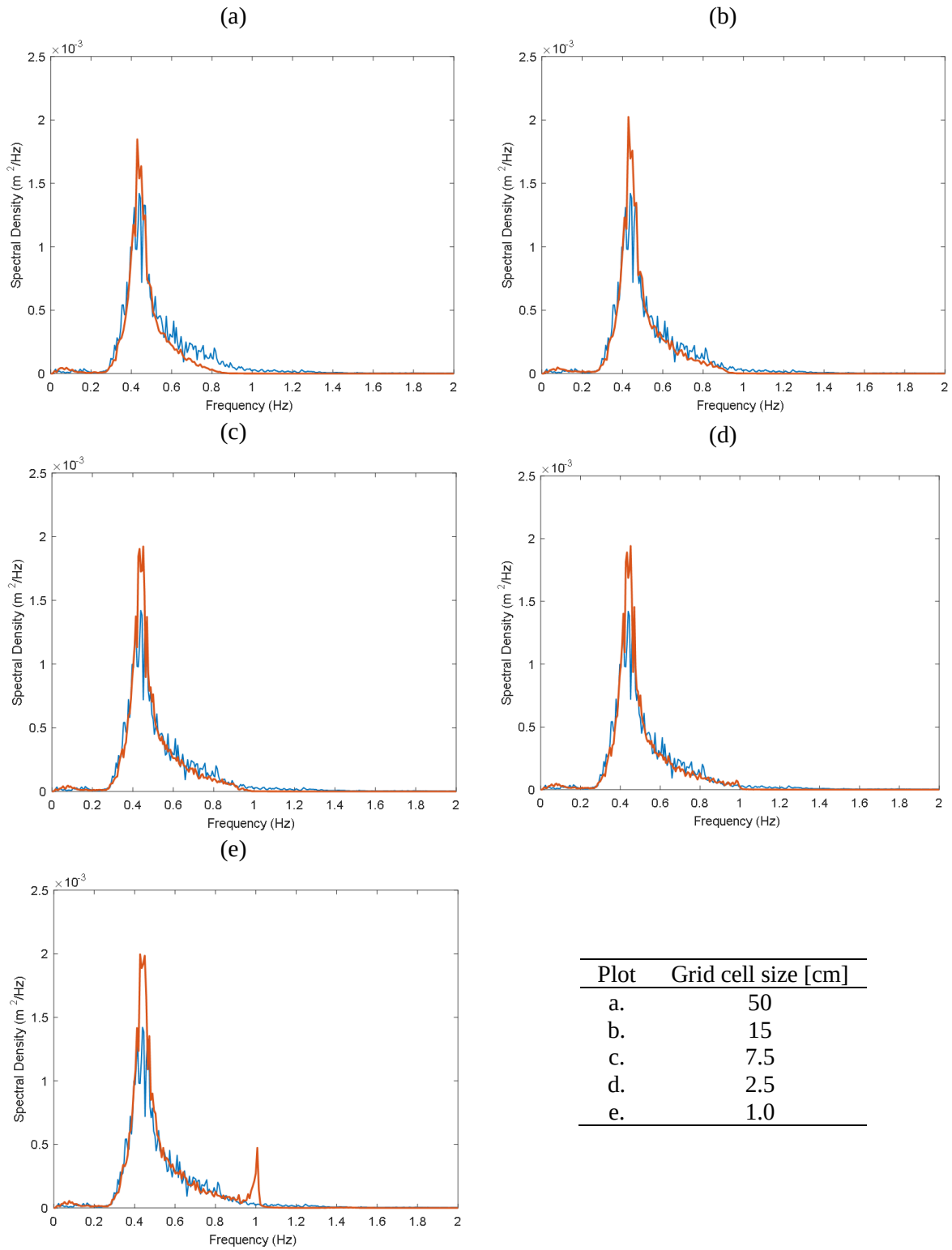

Plot	Grid cell size [cm]
a.	50
b.	15
c.	7.5
d.	2.5
e.	1.0

Figure 40. Grid size analysis for test 5 at position 1. Orange line is the SWASH spectrum and the blue line is the observed spectrum.

From the combination of the error, visual comparison with the measured spectrum and the runtime, two results are selected as optimal. It is opted for a grid cell size of 2.5cm (2600 cells) and 7.5cm (1000 cells) because these two have little change in results, to be carried on to the next step of the sensitivity analysis.

Layer analysis

Similar to the grid size. the number of layers is analysed. This is done for the two selected grid sizes of 2.5cm and 7.5cm. Again, this is done for all test numbers. The results are averaged and is summarized in Table 7 and Table 8. This analysis is only done up to three layers. This is because the difference between two and three layers in results is minimal, but the runtime increases exponentially. For this research. it is concluded that two layers suffices. The SWASH manual gives a simple calculation for the number of layers, which depends on the kd value. In this case, for a water depth of 0.96m and a wave number k of 0.133, kd becomes 0.13. The SWASH manual suggests that either 1 layer suffices, with a 3% error, or 2 layers with a 1% error for a kd value lower than 7.7.

Table 7. Layer analysis for grid size 7.5cm.

Number of layers	Runtime [min]	Position 1 (x=3.415m) Error H_{m0} [%]	Position 2 (x=15.54m) Error H_{m0} [%]
1	3	-0.74	-2.92
2	9	0.27	-0.40
3	16	0.34	-0.98

Table 8. Layer analysis for grid size 2.5cm.

Number of layers	Runtime [min]	Position 1 (x=3.415m) Error H_{m0} [%]	Position 2 (x=15.54m) Error H_{m0} [%]
1	8	0.28	-1.47
2	41.5	1.08	0.76
3	216.5	1.28	0.33

From this analysis, it is concluded that a grid size of 7.5cm, or 100 cells per wave length in combination with two layers, suffices, as was expected by the SWASH manual, Visually. the plots are all very similar, so only the chosen one is presented in Figure 41.

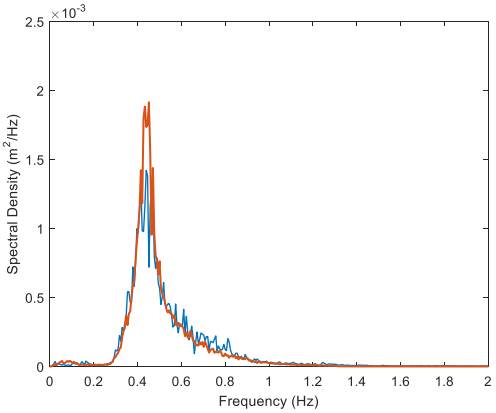

Figure 41. Spectral analysis for a SWASH model with 7.5cm grid cells and 2 layers. Spectral plot from test 5.

Appendix 2: Calibration of SWASH.

Before the actual calibration, the model is run with default options.

Default SWASH analysis

For the selected grid size and layers, eleven SWASH runs have been executed with the different input parameters. In Table 9, a comparison is shown between the wave heights observed by the lab test and the wave heights simulated by SWASH for the same input. This is examined once near the wave maker and twice near the dike, at 45.54m and at 45.96m distance from the wave maker.

Table 9. Results total wave heights H_{m0} first sensitivity analysis.

Test	Wave maker (3.415m)		Dike (45.54m)		Dike (45.96m)	
	Observed H_{m0} [m]	SWASH H_{m0} [m]	Observed H_{m0} [m]	SWASH H_{m0} [m]	Observed H_{m0} [m]	SWASH H_{m0} [m]
1	0.0545	0.0566	0.045	0.0412	0.0511	0.0457
2	0.0476	0.0483	0.0413	0.0379	0.0457	0.042
3	0.0509	0.0495	0.0419	0.0383	0.0535	0.0424
4	0.0508	0.0522	0.0376	0.0399	0.0421	0.0449
5	0.0642	0.0669	0.048	0.0454	0.0557	0.0498
6	0.0555	0.0574	0.0397	0.0421	0.0433	0.047
7	0.0972	0.0994	0.0574	0.0573	0.061	0.0614
8	0.1185	0.1198	0.0629	0.064	0.0667	0.0675
9	0.0684	0.0683	0.0559	0.046	0.0635	0.0503
10	0.0651	0.0649	0.0544	0.0446	0.062	0.0489
11	0.1125	0.1129	0.0694	0.0618	0.084	0.0653

For this sensitivity, two initial things are taken into account. For starters the performance target diagram, on which the SCI and Rel.bias for the wave heights are examined.

Looking at the total wave height H_{m0}, it can be concluded that the software performs very well for the initial wave profile near the wave maker (SCI=0.02173 and Rel.bias=0.01401). However, closer near the dike, the performance decreases and actually underpredicts the results (SCI=0.15993 and Rel.bias=-0.10086).

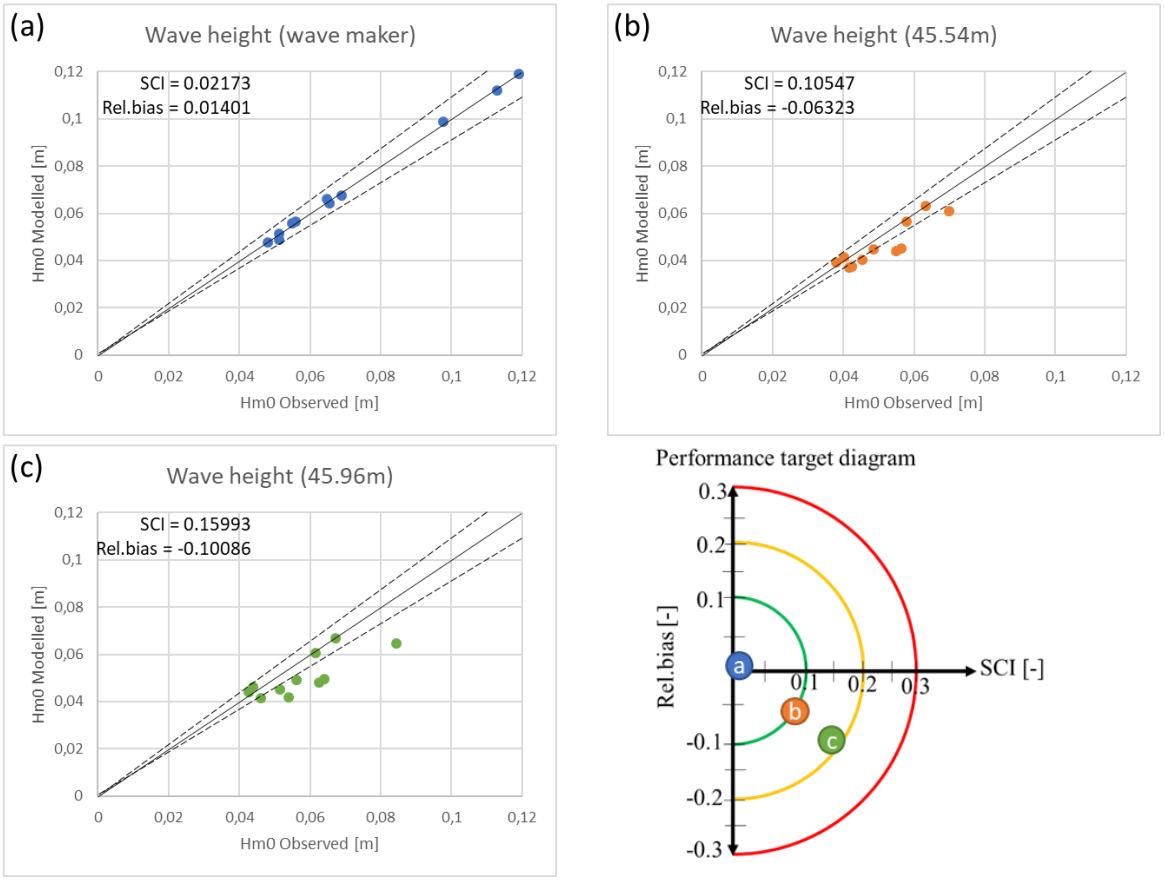

Figure 42. Results first sensitivity analysis. The plots show the wave heights H_{m0} and compare the observed and the SWASH values.

Next, the wave height is split up in a high frequency component and a low frequency component. This is first compared near the wave maker.

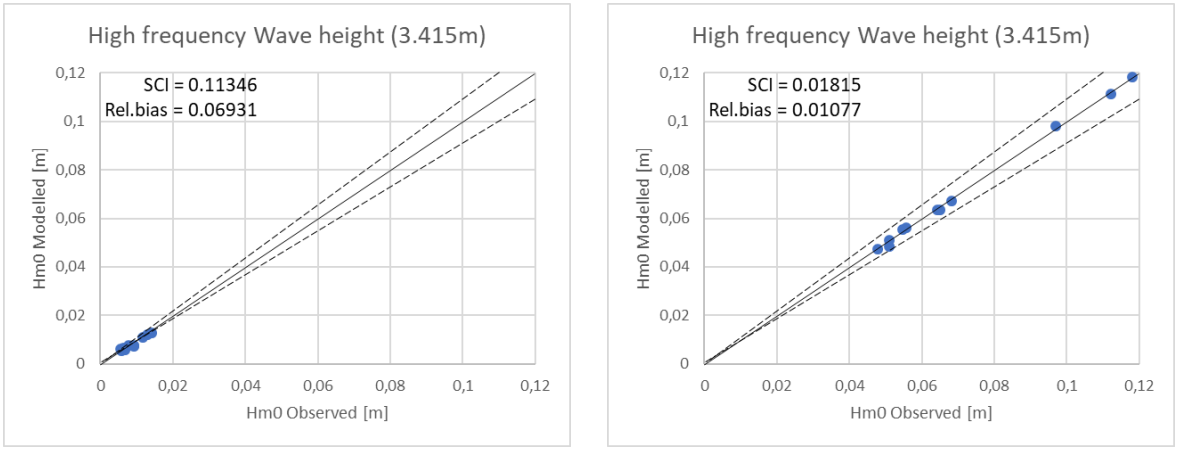

Figure 43. First sensitivity analysis near the dike. Left the low frequency wave height and right the high frequency wave height.

As was seen in the analysis of the total wave height, the model also performs excellent near the dike when dividing the wave heights in low and high frequency components.

This same analysis is done for the wave heights near the dike. The results are presented in Figure 44:

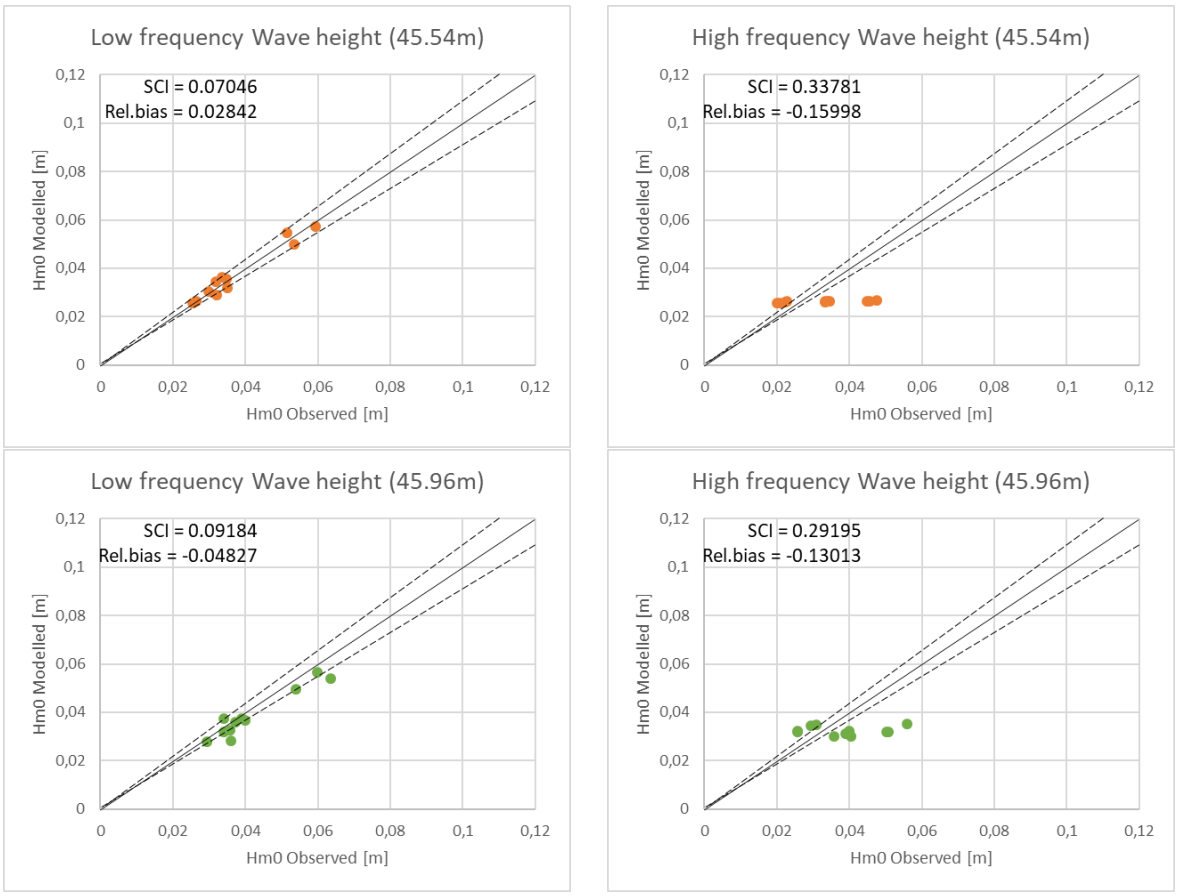

Figure 44. Performance of SWASH near the dike. Top plots at x=45.54m, bottom plots at x=45.96m. Left plots show the low frequency wave height, right show the high frequency wave height.

What immediately stands out is that there is some sort of frequency cut-off in the high frequencies. The software seems to perform well on the lower frequencies at the two locations, but less good at the high frequencies, as can also be seen from the plotted wave spectra. Near the wave maker, the spectra are almost identical, but near the dike, the higher frequencies are under-predicted.

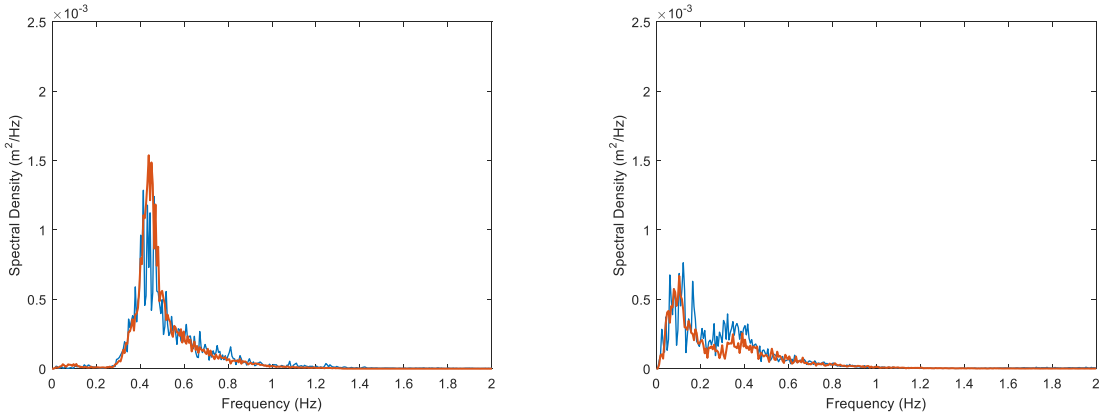

Figure 45. Wave spectra for test 1. Left near the wave maker, right near the dike. Orange line is the SWASH spectrum and the blue line is the observed spectrum.

Finally, the IGC is compared for all three cases. It can be easily seen that there is some inaccuracy in the software at the moment. The performance at the wave maker is almost acceptable (SCI = 0.13332, Rel.bias= 0.07999) but can be more accurate. The biggest problem here is that the short gravity waves are simulated well, but the low frequency is overestimated.

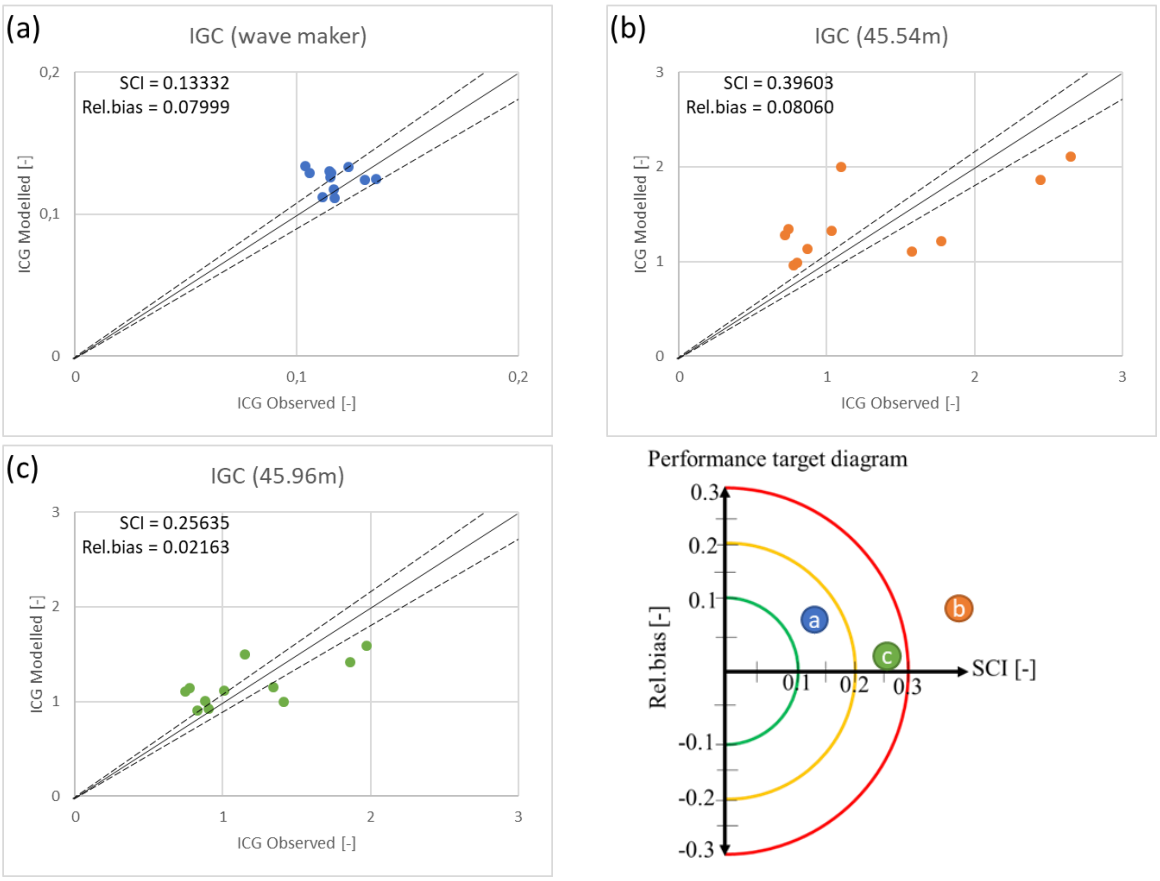

Figure 46. Results first sensitivity analysis. The plots show the IGC and compare the observed and the SWASH values.

Near the dike, the results are very scattered and show no pattern. With the SCI_b = 0.39603 and SCI_c = 0.25635, this is considered unacceptable. The main problem is that the low frequency waves are not simulated accurately near the dike.

Breaker parameters

To make the SWASH model more accurate, the breaker parameters α and β are varied. First of all, the values for α are gradually increased from 0.6 to 1.0 (maximum). This analysis is done for all tests. Near the wave maker, the waves are assumed not to be breaking. The wave heights near the wave maker were checked and did not change with the variation of this parameter. The results presented in the Table 10 are the deviations between the observed values and the SWASH values. They are presented as the averaged value of all tests near the two locations at the dike. The wave heights are examined in total and as separated between high and low frequency.

Table 10. Sensitivity breaker parameter α, deviation errors

α [-]	Location 1 (45.54m) Deviation [%]			Location 2 (45.96m) Deviation [%]		
	H_{m0}	H_{m0LF}	H_{m0HF}	H_{m0}	H_{m0LF}	H_{m0HF}
0.6	-8.27	6.89	-27.09	-14.47	-7.31	-23.00
0.7	-6.93	8.08	-35.48	-15.33	-6.77	-21.32
0.8	-6.19	8.60	-34.41	-14.66	-6.30	-20.35
0.9	-5.83	8.89	-33.88	-14.24	-5.96	-19.76
1.0	-5.77	8.80	-33.53	-14.28	-6.13	-19.64

From this table, it can be seen that varying the breaker parameter α has some, yet limited effect. With some exceptions, the deviation was optimal for a breaker parameter of 0.9, although not much variation can be noticed for between parameters higher than 0.7. For now, α=0.9 is assumed and parameter β is varied. The default value is 0.3 and α > β. Similar to α, the results are presented in Table 11, similar to the analysis of breaker parameter α:

Table 11. Sensitivity breaker parameter β, deviation errors.

β [-]	Location 1 (45.54m) Deviation [%]			Location 2 (45.96m) Deviation [%]		
	H_{m0}	H_{m0LF}	H_{m0HF}	H_{m0}	H_{m0LF}	H_{m0HF}
0.4	2.51	19.69	-18.34	4.50	10.61	-2.61
0.5	2.58	19.36	-17.58	4.38	7.76	-2.49
0.6	2.87	19.41	-16.91	4.44	10.08	-2.01
0.7	3.20	19.77	-16.77	5.06	10.56	-1.29
0.8	3.56	20.19	-16.36	5.46	11.20	-1.03

The introduction of the β parameter has an immediate effect on the simulation. Although the low frequency wave height become significantly worse, the high frequency wave height show a very large improvement. At location 1, the accuracy is doubled (although still not very accurate) and at location 2 the error becomes negatable. The low frequency wave heights are very susceptible to bottom friction, therefore, a breaker parameter β of 0.6 is chosen and the low frequency wave heights are ignored in this decision.

Bottom friction

Next, bottom friction is introduced. This is done by using a Manning coefficient [$m^{-1/3}s$], and is varied from 0.00 to 0.04. As friction possibly influences the wave height near the wave maker too, it is implemented in this analysis. The wave heights are analysed using a deviation error, and are split up into their high and low frequency components. The results here are the averaged values of all tests.

Table 12. Sensitivity friction coefficient, deviation errors.

Manning Coeff. [$m^{-1/3}s$]	Wave maker Deviation [%]			Dike (45.54m) Deviation [%]			Dike (45.96m) Deviation [%]		
	H_{m0}	H_{m0LF}	H_{m0}	H_{m0}	H_{m0LF}	H_{m0}	H_{m0}	H_{m0LF}	H_{m0HF}
0.005	5.30	16.44	5.17	4.58	-4.08	12.80	1.08	5.30	16.44
0.010	5.14	12.33	5.02	3.13	-6.12	11.61	5.57	5.14	12.33
0.020	4.52	0.13	4.55	-1.67	-12.24	8.33	1.97	4.52	0.05
0.030	3.74	-20.55	3.92	-14.38	-20.70	3.27	-4.67	3.74	-20.55
0.040	3.27	-38.36	3.61	-14.38	-29.45	-1.19	-12.03	3.27	-38.36

Appendix 3: Froude scaling

The whole validation of the model was done in a lab scale of 1:25. To scale up the model, there isn't any physical data to compare with to validate the model again. Therefore, the observed results from the lab experiment are theoretically scaled up and compared to see if the results are still similar. To do the scaling, the Froude scale is used (Heller, 2011). An overview of the changing parameters is given in Table 13, in example of test 5.

Table 13. Scale parameters

Parameter	Lab scale	Full scale
Scale	1	25
Wave height [m]	0.0668	1.67
Wave period [s]	2.2979	11.4895
Grid size [m]	0.075	1.875
Grid cells	850	850
Duration [min]	36	180
Friction [$m^{-1/3}s$]	0.02	0.02

The results of the SWASH model are compared to the scaled up lab observations. This is done for all tests, but only the results for test 5 are presented in Table 14. It can be concluded that the results of the full-scale SWASH model are very similar to the small scale and are also very similar to the theoretically scaled up lab observations. Therefore, it is concluded that the model is still valid on full scale.

Table 14. Example full scale (test 5).

Manning Coeff. [$m^{-1/3}s$]	Wave maker Wave heigh [m]			Dike (45.54m) Wave heigh [m]			Dike (45.96m) Wave heigh [m]		
	H_{m0}	H_{m0LF}	H_{m0}	H_{m0}	H_{m0LF}	H_{m0}	H_{m0}	H_{m0LF}	H_{m0HF}
SWASH	1.6882	0.2716	1.6666	1.2599	1.0038	0.7445	1.4834	1.0149	1.0544
Lab (scaled up)	1,6050	0,1825	1,5950	1,2000	0,8575	0,8400	1,3925	0,9850	0,9850

Appendix 4. Analysis of the water level and wave heights.

The wave heights and water levels are given here. Without vegetation, there are 125 simulations, which each could have a separate analysis of the water level and wave height. This would be too much to depict here. Therefore two random results are chosen and the cross-shore evolution is shown. The two random results are a slope of 1:500 with a period T_P=10s (Figure 47); and a slope of 1:100 with a period T_P=8s (Figure 48).

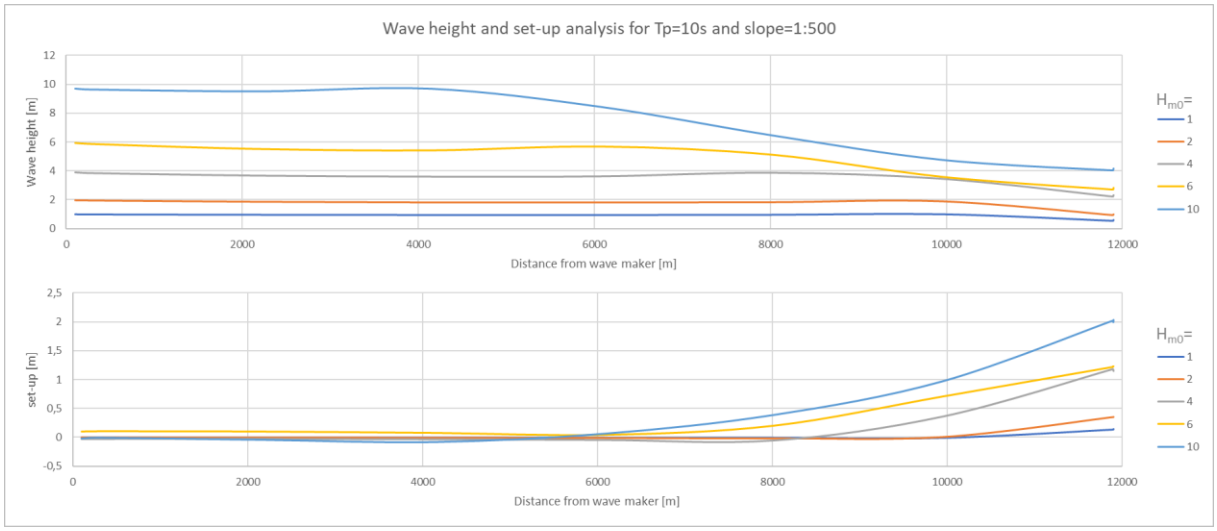

Figure 47. Wave height (top) and water level set-up (bottom) analysis for T_P=10s and slope=1:500.

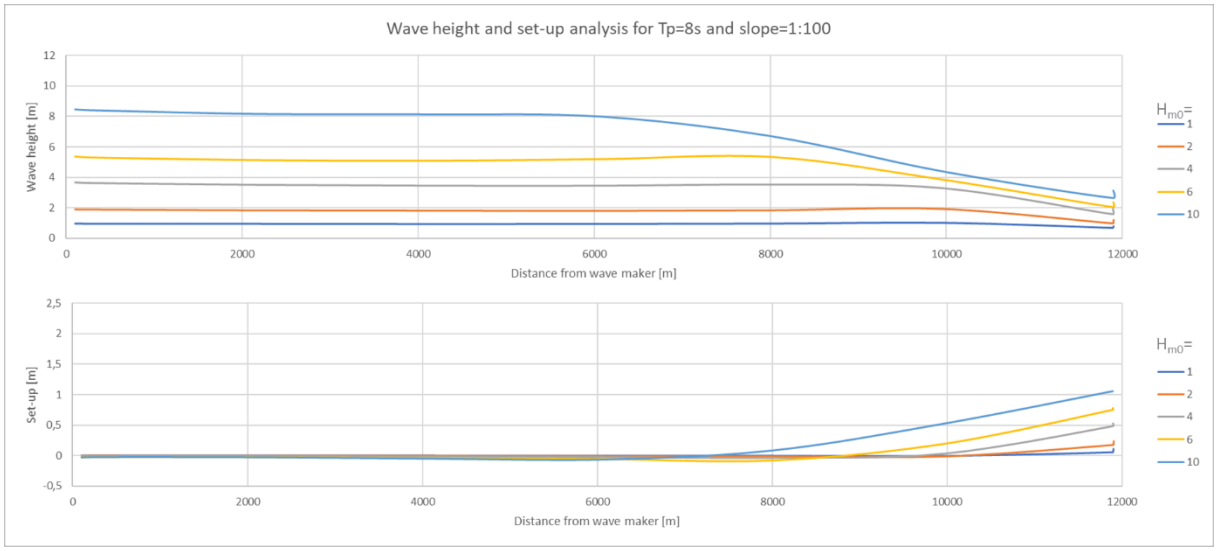

Figure 48. Wave height (top) and water level set-up (bottom) analysis for T_P=8s and slope=1:100.

The full analysis of the set-up at the dike toe is done here and summarized in the main report. The set-up at the dike toe is analysed first. This is done by taking the mean value of the water level elevation time series. The still-water level (without set-up) at the toe of the dike is constant at 1m for all simulations. The output can be seen in Table 15 to Table 19.

Some trends can be noticed. First of all, the effect of the slope is that the set-up becomes larger for weaker slopes. This effect is enlarged with increasing wave heights. For the smallest wave height, the difference of wave heights for different slopes is minimal. The effect of the wave height is very linear, showing increased set-up for larger wave heights. The same can be concluded for the periods, showing increased set-up for longer periods.

Table 15. Output water set-up [m] at the dike toe for a 1:25 slope.

T_P [s]	Set-up [m]				
	1	2	4	6	10
6	0.124	0.181	0.308	0.429	-
8	0.142	0.237	0.404	0.506	0.645
10	0.169	0.281	0.264	0.602	0.659
12	0.180	0.275	0.521	0.592	0.834
14	0.190	0.300	0.522	0.660	0.913

Table 16. Output water set-up [m] at the dike toe for a 1:50 slope.

T_P [s]	Set-up [m]				
	1	2	4	6	10
6	0.097	0.097	0.298	0.448	-
8	0.110	0.220	0.460	0.689	0.769
10	0.134	0.261	0.494	0.747	0.904
12	0.137	0.298	0.516	0.779	0.967
14	0.152	0.293	0.530	0.786	1.003

Table 17. Output water set-up [m] at the dike toe for a 1:100 slope.

T_P [s]	Set-up [m]				
	1	2	4	6	10
6	0.078	0.140	0.265	0.507	-
8	0.108	0.240	0.510	0.752	0.904
10	0.130	0.269	0.591	0.796	0.999
12	0.138	0.299	0.610	0.797	1.060
14	0.159	0.341	0.625	0.842	1.101

Table 18. Output water set-up [m] at the dike toe for a 1:200 slope.

T_P [s]	Set-up [m]				
	1	2	4	6	10
6	0.060	0.118	0.373	0.663	-
8	0.108	0.233	0.605	0.979	1.168
10	0.131	0.303	0.798	1.058	1.264
12	0.141	0.373	0.819	1.073	1.331
14	0.173	0.373	0.823	1.087	1.486

Table 19. Output water set-up [m] at the dike toe for a 1:500 slope.

T_P [s]	Set-up [m]				
	1	2	4	6	10
6	0.032	0.055	0.209	0.967	-
8	0.096	0.225	0.656	1.311	2.310
10	0.138	0.352	1.150	1.504	2.029
12	0.163	0.449	1.258	1.503	1.733
14	0.178	0.501	1.296	1.504	1.846

Appendix 5. Seiching.

A seiche can be defined as a standing wave in a closed environment (Roeber and Bricker, 2015). The simulation can be seen as a closed environment. If the seiche period of this system is equal to the time a wave needs to travel from the wave maker to the dike and back, it can be concluded that seiching occurs for a certain period. This is calculated to determine whether the T_P peak at 10s for several contour plots is due to seiching or another explanation needs to be found.

The seiche period of the system is defined as:

$$T_{seiche} = \frac{2L}{n\sqrt{gh}} \qquad (A.1)$$

Where: L = system length [m]

n = number of nodes in a system, here n=1

g = gravitational acceleration = 9.81 m/s²

h = water depth [m]

Because this peak seems to originate at the 1:100 slope, this is done for this system. The seiche period T_{seiche}=472s. The time a wave needs to travel from the wave maker to the dike and back is calculated by determining the wave celerity at a certain number of cells. Knowing the size of each cell, the time for a wave to cross the cell can be determined. The sum of all these equal the time it takes for a wave to reach the dike. This duration times two is the total time needed to compare with the seiche period of the system. However, this results in a duration of 552s, which is not equal to the seiche period. Therefore, seiching is not the reason for this peak.